Tectonophysics 683 (2016) 109–123

Contents lists available at ScienceDirect

Tectonophysics

journal homepage: www.elsevier.com/locate/tecto

Thermal and structural evolution of the external Western Alps: Insights from (U–Th–Sm)/He thermochronology and RSCM thermometry in the Aiguilles Rouges/Mont Blanc massifs

A. Boutoux [a,*], N. Bellahsen [a], U. Nanni [a], R. Pik [b], A. Verlaguet [a], Y. Rolland [c], O. Lacombe [a]

[a] Sorbonne Universités, UPMC Univ Paris 06, CNRS, Institut des Sciences de la Terre de Paris (iSTeP), 4 place Jussieu, 75005 Paris, France
[b] CRPG, Université de Lorraine, CNRS, 7358, F-54501 Vandoeuvre-Lès-Nancy, France
[c] Géoazur, Université de Nice Sophia-Antipolis, CNRS, UMR 7329, Valbonne, France

ARTICLE INFO

Article history:
Received 7 January 2016
Received in revised form 15 April 2016
Accepted 4 June 2016
Available online 11 June 2016

Keywords:
External Alps
(U–Th–Sm)/He on zircon
RSCM
Collision
Thermal peak
Crustal ramps

ABSTRACT

In the Western Alps, the External Crystalline Massifs (ECM) are key places to investigate the kinematics and thermal structure of a collisional crustal wedge, as their paleo-brittle/ductile transition is now exhumed at the surface. New (U–Th–Sm)/He data on zircon and new Raman Spectroscopy on Carbonaceous Material (RSCM) data from the Aiguilles Rouges and the Mont Blanc massifs, coupled to HeFTy thermal modeling, constrain the thermal evolution and exhumation of the massifs. In the cover of the Aiguilles Rouges massif, we found that the maximal temperature was about 320 °C (+/−25 °C), close to the maximal temperature reached in the cover of the Mont Blanc massif (~350 °C +/− 25 °C). We show that, after a fast heating period, the thermal peak lasted 10–15 Myrs in the Mont Blanc massif, and probably 5–10 Myrs in the Aiguilles Rouges massif. This thermal peak is synchronous with crustal shortening documented in the basement. (U–Th–Sm)/He data and thermal modeling point toward a coeval cooling of both massifs, like other ECM, at around 18 Ma +/−1 Ma. This cooling was related to an exhumation due to the initiation of frontal crustal ramps below the ECM, quite synchronously along the Western Alps arc.

© 2016 Elsevier B.V. All rights reserved.

1. Introduction

Crustal and lithospheric rheology drives the interactions between the structural and the thermal evolution of collisional wedges. Building realistic models of crustal wedge evolution therefore requires a detailed knowledge of thermal evolution through space and time. Thermobarometric, thermochronological, and geochronological data are key constraints for such an analysis. In the Western Alps (Fig. 1), a wealth of data is available to discuss shortening and cooling sequences. During the collision, the proximal part of the European margin and its inherited structures were partially underthrusted, hence buried under the internal Penninic units (e.g., Bellanger et al., 2015). In the external zone below the Penninic Frontal Thrust, the External Crystalline Massifs (ECM) consist of basement units exposing the Alpine Oligo-Miocene brittle–ductile transition of the European crust (Fig. 1). Thus, they constitute key places to study the crustal evolution of the Alpine collisional wedge as they provide insights into processes operating at mid-crustal levels.

The geometry of the Alpine collisional wedge can be partly constrained South of the Aiguilles Rouges and the Mont Blanc massifs thanks to the ECORS profile (e.g., Nicolas et al., 1990; Guellec et al., 1990). Moreover, the amount of thermochronological (e.g., Glotzbach et al., 2008, 2011), geochronological (Leloup et al., 2005; Rolland et al., 2008; Cenki-Tok et al., 2013; Egli et al., 2016), and thermobarometric data (Rolland et al., 2003; Rossi et al., 2005) now provide a good understanding of the pressure and temperature (P–T) peaks and cooling history of the Mont Blanc massif. Yet, West of the Mont Blanc massif, in the Aiguilles Rouges massif, both P–T peak and cooling history are still unconstrained. Therefore, the sequence of shortening and exhumation in the Alpine crustal wedge is still debated. For some authors, Mesozoic inherited syn-rift basins in the ECM were inverted with "thick-skinned" shortening style (e.g., the Oisans basins, Butler et al., 2006; Bellahsen et al., 2012, 2014; Boutoux et al., 2014; Bellanger et al., 2014, 2015; the Morcles nappe, Escher et al., 1993; Burkhard and Sommaruga, 1998). For others, the ECM cover was shortened with a "thin-skinned" style before stacking of basement units (Leloup et al., 2005). These two models have opposite implications in terms of rheology as shortening style may be controlled by inherited lithosphere thermicity (e.g., Mouthereau et al., 2013). It is therefore of primary interest to acquire new high-resolution constraints on the thermobarometric

* Corresponding author at: Université Pierre et Marie Curie, ISTeP, UMR 7193 UPMC-CNRS, Case 129, T46-00, 2eme étage, 4 place Jussieu, 75252 Paris cedex 05, France.
E-mail address: alexandre.boutoux@upmc.fr (A. Boutoux).

http://dx.doi.org/10.1016/j.tecto.2016.06.010
0040-1951/© 2016 Elsevier B.V. All rights reserved.

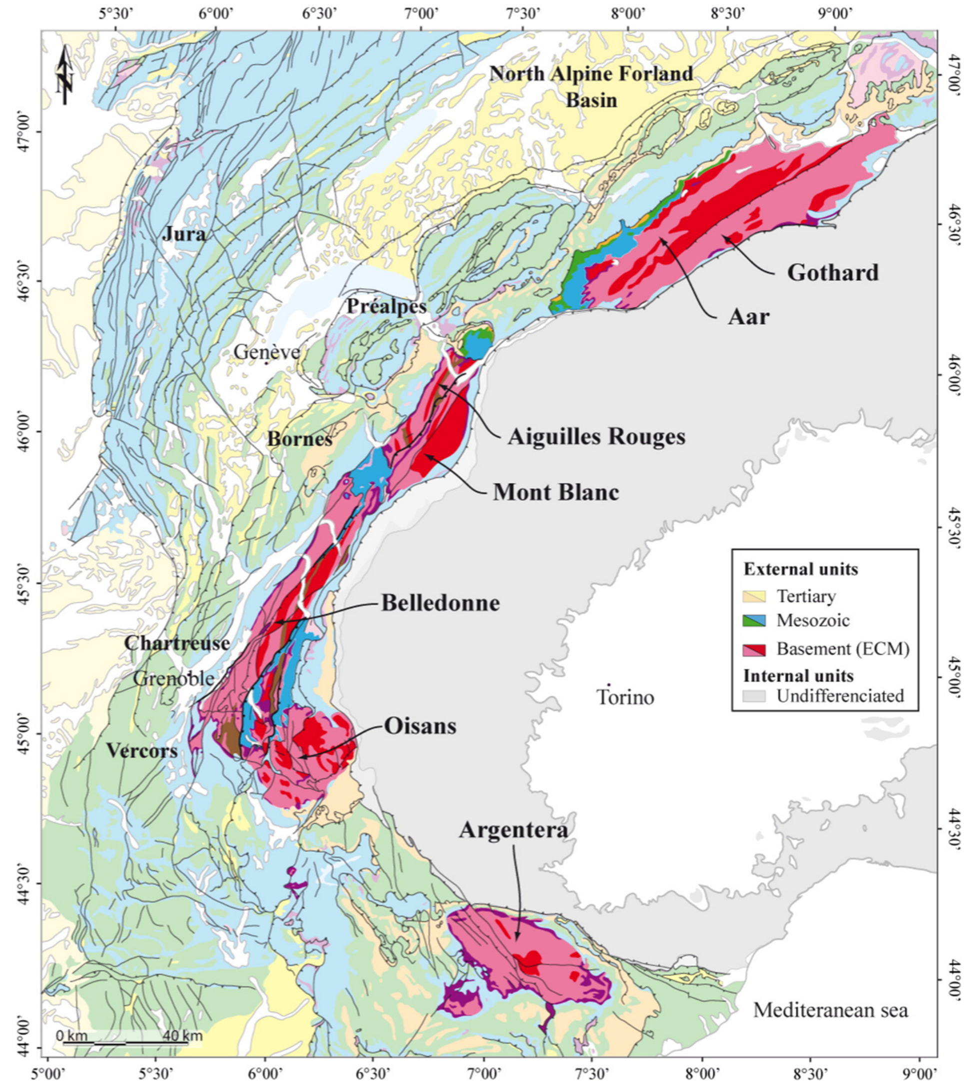

Fig. 1. Geological map of the Alpine western arc external units, highlighting the basement of the European proximal margin (the External Crystalline Massifs) and the sedimentary cover of its inherited basins (the Oisans basins, the Mont-Joly nappe, the Morcles nappe and the Doldenhorn nappe).

evolution of both the cover and the basement of tectonic units in the External Crystalline Massifs.

Recently, Bellanger et al. (2015) showed that the Oligocene temperature peak in the external southwestern Alps (Oisans massif) was quite constant over half the width of the collisional wedge (around 75 km). In the external northwestern Alps, the lack of thermobarometric data in the Aiguilles Rouges massif does not allow us to decipher the Oligo-Miocene thermal structure. In this contribution, we provide new Raman Spectroscopy on Carbonaceous Material (RSCM) thermometric data to document the thermal peak reached by the Aiguilles Rouges and the Mont Blanc massifs. Moreover, we also obtained new Low-Temperature (LT) thermochronological data ((U–Th–Sm)/He on zircon, ZHe) on basement rocks from both the Aiguilles Rouges and the Mont Blanc massifs to constrain the cooling/exhumation history. Ultimately, the combination of these new data with already published ones provides a better understanding of the thermo-tectonic behavior of the crust during continental collision in Alpine-type orogens.

2. Geological setting

The Mont Blanc and the Aiguilles Rouges massifs (Figs. 1, 2) are parts of the External Crystalline Massifs. Both massifs consist of early Paleozoic paragneiss, orthogneiss and migmatites (e.g., Frey et al., 1999; von Raumer and Bussy, 2004) dated at 453 Ma +/− 3 Ma in the Mont Blanc massif (U—Pb dating on zircon, Bussy and von Raumer, 1994). During the Late Carboniferous, they were intruded at mid-crustal level by magmatic bodies (von Raumer et al., 2009). The Mont Blanc granite is a mobile calc-alkaline anatectic batholith emplaced at 304 Ma (Bussy and von Raumer, 1994). In the Aiguilles Rouges massif and in the western part of the Mont Blanc massif, the Vallorcine and the Montenvers vertical sheet-like intrusions are emplaced synchronously at 306 +/− 1.7 Ma (Brändlein et al., 1994; Bussy et al., 2000).

The Mont Blanc massif forms a pop-up structure, bounded by two main tectonic features: the Mont Blanc Shear Zone (MBSZ) on its northwestern part and the Mont Blanc Back-Thrust (MBBT) on its southeastern part (Leloup et al., 2005; Rolland et al., 2008; Egli and Mancktelow, 2013) (Fig. 3). The inner part of the massif is structured by narrow (1–50 m), steep and transpressional (dextral) alpine shear zones separating lower strain domains (100–500 m). The shear zones are arranged in a fan-like geometry (Bertini et al., 1985) and oriented in two conjugate N–S to NE–SW sets with striae-lineations featuring horizontal NW–SE compression with a component of dextral strike-slip movement (Rolland et al., 2003, 2008; Rossi et al., 2005). Alpine P–T peak in the Mont Blanc massif is estimated at 5 +/−0.5 kbar and 400 +/− 25 °C from thermobarometric analysis of syn-kinematic phases in alpine shear zones (Rolland et al., 2003; Rossi et al., 2005).

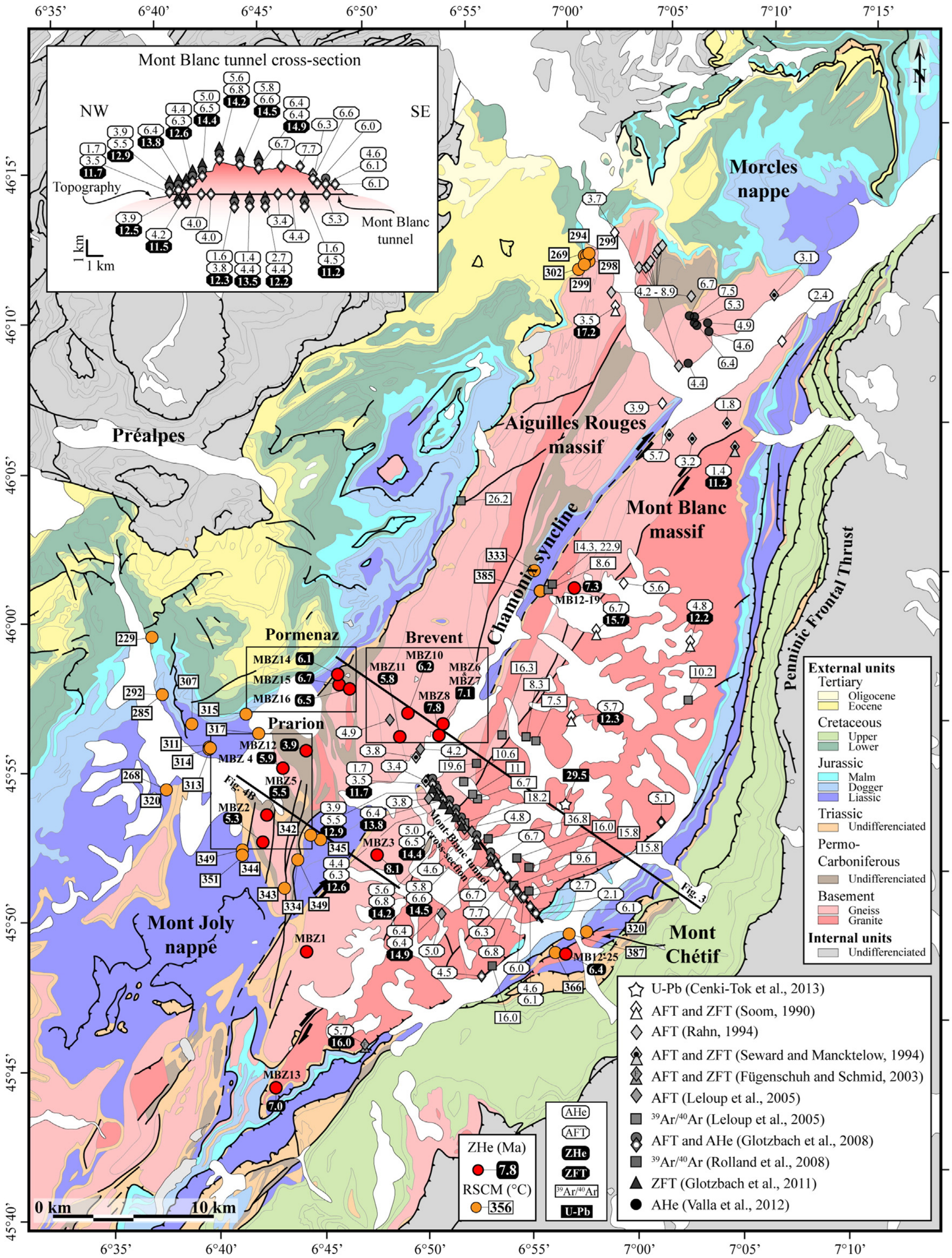

Fig. 2. Geological map of the Mont Blanc and Aiguilles Rouges basement massifs area and cross-section of the Mont Blanc massif with the thermochronological (ZFT, AFT, AHe; Rahn, 1994; Seward and Mancktelow, 1994; Fügenschuh and Schmid, 2003; Leloup et al., 2005; Glotzbach et al., 2008, 2010) and direct dating ($^{40}Ar/^{39}Ar$; Leloup et al., 2005; Rolland et al., 2008) data available in literature, as well as ZHe and Raman data from this study.

Two stages of deformation and fluid–rock interaction are recorded in the massif (see Rolland and Rossi, 2016 for a synthesis). The oldest shear zones (stage 1) are dated at 29–30 Ma (Fig. 2) constrained by U—Pb dating (Cenki-Tok et al., 2013). These shear zones were formed during or at the end of the ECM burial like in the Oisans-Pelvoux Massif (Fig. 1, Simon-Labric et al., 2009; Bellanger et al., 2015). More recent shear zones (stage 2) are dated mostly from 22 Ma to 14 Ma (Fig. 2; $^{40}Ar/^{39}Ar$ dating, Rolland et al., 2008), and horizontal veins are dated between 15 and 11 Ma ($^{40}Ar/^{39}Ar$ dating of adularia; Rossi and Rolland, 2014). Exhumation is recorded in the Mont Blanc massif by LT thermochronological data: zircon fission track (ZFT) ages are between 11.2 Ma and 16 Ma (Fig. 2; Seward and Mancktelow, 1994; Fügenschuh and Schmid, 2003; Glotzbach et al., 2011); apatite fission track (AFT) ages are between 1.8 Ma and 6.8 Ma (Fig. 2; Soom, 1990;

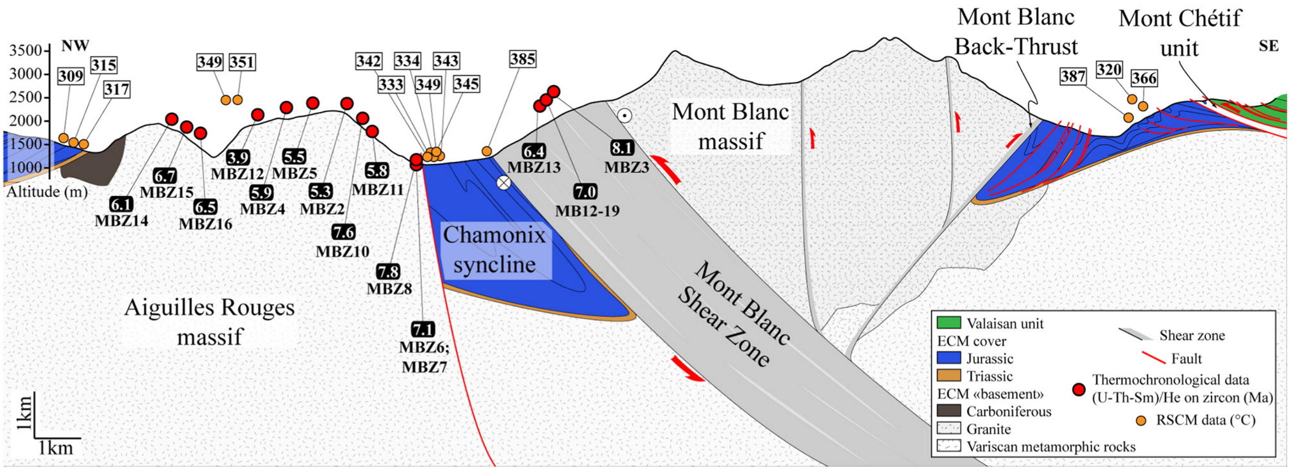

Fig. 3. Cross-section of the Aiguilles Rouges and Mont-Blanc massifs (see Fig. 2 for location). Dots indicate the location of samples used in this study.

Seward and Mancktelow, 1994; Fügenschuh and Schmid, 2003; Leloup et al., 2005; Glotzbach et al., 2008); (U—Th-Sm)/He on apatite (AHe) ages range from 1.4 Ma to 6.4 Ma (Fig. 2; Glotzbach et al., 2008).

In the Aiguilles Rouges massif, P–T peak is dimly constrained although fluid inclusion studies of parautochonous cover of the massif indicate a minimal temperature about 275 °C (Mullis, 1975). Only few LT thermochronological data are available on the Aiguilles Rouges massif: one ZFT age is at 17.2 Ma (Soom, 1990), while others are non reset (Vernon et al., 2008); AFT ages range between 3.1 Ma and 8.9 Ma (Fig. 2; Rahn, 1994; Seward and Mancktelow, 1994; Leloup et al., 2005); AHe ages are between 4.4 Ma and 6.7 Ma (Fig. 2; Valla et al., 2012). Small alpine shear zones are observed in the northern part of the massif. The youngest ones are dated at 14–18 Ma, constrained by $^{40}Ar/^{39}Ar$ dating (Egli, 2013) and the oldest one are dated at 30 Ma (Rb—Sr dating, Egli et al., 2015).

The Morcles nappe is usually interpreted as the cover of the Mont Blanc massif (Escher et al., 1993) and is composed of Triassic to Cretaceous metasedimentary rocks (Fig. 2). This nappe is a large recumbent anticline, presenting a highly sheared reverse limb (Ramsay et al., 1983) over the Aiguilles Rouges massif. For most authors, the reverse limb shear zone thus roots in the Chamonix syncline (Escher et al., 1993; Bauville et al., 2013), interpreted as an inverted inherited syn-rift basin (Steck et al., 1997; Burkhard and Sommaruga, 1998; Boutoux et al., 2014). Alternatively, the Morcles nappe may root East of the Mont Blanc massif (Leloup et al., 2005). Further South, the Mont Joly nappe (Fig. 2) is interpreted as the southern equivalent of the Morcles nappe, rooting in the Chamonix inherited basin (Epard, 1990; Bellahsen et al., 2014).

The North Alpine Foreland Basin (NAFB, Fig. 1; Sinclair, 1997; Ford et al., 2006) developed during Oligo-Miocene times. This molasse basin was deformed by thrusts linked to basement ramps below the Aiguilles Rouges massif (Burkhard and Sommaruga, 1998). During late Miocene times, the youngest alpine thrusts initiated below this massif, propagated below the NAFB in the Triassic evaporites and activated the Jura fold-and-thrust-belt (Becker, 2000). The Jura décollement and the NAFB were subsequently deformed by later high-angle basement thrusts related to inversion of Permo-Carboniferous basins (e.g., Lacombe and Mouthereau, 2002 and references therein).

Because of the lack of thermochronological data in the Aiguilles Rouges massif, the sequence of shortening is still debated. Leloup et al. (2005) proposed that the Aiguilles Rouges massif was exhumed first and that the Mont Blanc massif was emplaced later and out-of-sequence. However, Burkhard and Sommaruga (1998) suggested that the initiation of the basement thrusts occurred in-sequence. One goal of this contribution is to document the thermal peak and cooling of both the Aiguilles Rouges and Mont Blanc massifs in order to better constrain the shortening and exhumation sequence during the Alpine collision. We used Low Temperature thermochronology, (U–Th–Sm)/He on zircon (ZHe) to obtain data currently not available in the Mont Blanc and Aiguilles Rouges massifs. The ZHe system closure temperature (140–195 °C, Reiners et al., 2002) ranges between the AFT (95–160 °C, Gallagher et al., 1998) and the ZFT system closure temperatures (300–220 °C, e.g. Rahn et al., 2004; Garver et al., 2005; Bernet, 2009). Thus, ZHe data will further constrain the thermal evolution of the Mont Blanc and the Aiguilles Rouges massifs between 220 °C and 160 °C. Moreover, we obtained data with the Raman Spectroscopy of Carbonaceous Material methodology (RSCM) to constrain the thermal peak of the sedimentary cover of both Aiguilles Rouges and Mont Blanc massifs.

3. Methodology

3.1. Raman spectroscopy on carbonaceous material thermometry

Sampling for RSCM thermometry analysis was performed in the metasedimentary cover of both the Aiguilles Rouges and the Mont Blanc massifs in several areas distributed around the massifs (Figs. 2, 3). The metasedimentary cover consists of meta-marls rich in carbonaceous material (CM), from 0.1 to 4%, which permits the use of RSCM thermometry to estimate the maximal temperature attained by these rocks, indicated by the degree of graphitization of the CM.

With burial, heating, and subsequent metamorphism, the structure of CM trapped in these sediments gradually evolves toward graphite-like stable structures (Yui et al., 1996). This graphitization of CM is an irreversible process that therefore records the maximum temperature (T_{max}) experienced by the rocks during a P–T loop (Beyssac et al., 2002a, 2002b). The RSCM is based on the quantitative determination of the degree of graphitization of CM, measured from Raman Spectra (RS), which is a reliable indicator of metamorphic peak temperature. In a spectral window from 700 to 2000 cm^{-1}, the RS can be divided into a graphite band (G) and defect bands (D1, D2, D3, D4). The relative area of these bands reflects the degree of graphitization. It can be quantified using the R2 parameter, defined as the relative area of the main defect bands ($R2 = D1/(G + D1 + D2)$) (Beyssac et al., 2002b). These authors proposed an empirical thermometer, which links R2 to T_{max} for a temperature range of 330 to 640 °C with an intrinsic calibration error of 50 °C. At lower temperature (200–350 °C), the D3 and D4 bands are well developed. In this case, T_{max} can be estimated using the RA1 parameter ($RA1 = (D1 + D4)/(G + D1 + D2 + D3 + D4)$), with an intrinsic calibration error of 25 °C (Lahfid et al., 2010).

Raman spectra were obtained using a Renishaw InVIA Reflex microspectrometer (IMPMC, UPMC, France). Before each session, the spectrometer was calibrated with a silicon standard. We used a 514 nm Laser Physics argon laser in circular polarization and measurements were done on polished thin sections, following the analytical procedures described in Beyssac et al. (2002b, 2003) and Lahfid et al. (2010). 377 spectra were obtained on 28 samples (12 to 15 spectra per thin section) in extended scanning mode (700–2000 cm^{-1}). RS were post-processed using the software PeakFit, following the fitting procedures of both Beyssac et al. (2002b, 2003) and Lahfid et al. (2010). As our samples obviously experienced a T_{max} in the overlap range of both thermometers, T_{max} was determined for each sample from the mean peak ratio (R2 or RA1) calculated from the 12 to 15 spectra obtained for this sample, with the procedure giving the best fit.

3.2. (U–Th–Sm)/He low temperature thermochonology

Samples for ZHe thermochronology (Figs. 2, 3) consist of granites and gneisses that were collected in the southern part of the Aiguilles Rouges massif, in the western part of the Mont Blanc massif and in the Mont Chétif (Southeast of the Mont Blanc massif). In the Aiguilles Rouges massif, samples were collected along three different profiles (Brevent, Pormenaz and Prarion). The Brevent and the Pormenaz samples are aligned on a NW–SE section corresponding to the Mont Blanc tunnel (Fig. 2) between 1000 and 2200 m (Fig. 3). The Prarion samples are located on the southernmost part of the Aiguilles Rouges massif (Fig. 2) between 800 and 1800 m (Fig. 3).

Helium extraction and analyses were performed at the noble gas laboratory of the CRPG (Nancy, France). Zircon crystals were handpicked under binocular lens taking into account morphology, size and purity. Two or three single-grain replicates per sample were loaded into Pt capsules, degassed by oven at about 1500 °C during 20 min and analyzed for He concentrations with a VG-603 noble gas mass spectrometer (Pik et al., 2003; Godard et al., 2009; Tibari et al., 2016). U–Th–Sm content measurements were then carried out at the SARM (CRPG, Nancy, France). Zircon crystals and the opened Pt capsules were fused into Pt crucibles with ultra-pure $LiBO_2$ and $B(OH)_3$ for 2 h at 990 °C. The crucible, capsules and zircon samples were digested during 12 h before inductively couple plasma mass-spectrometer analysis (Vacherat et al., 2014; Tibari et al., 2016). The overall precision of He ages determined with this procedure is within 5–6% (1σ). Zircons with He content less than 1.10^{-13} mol and those for which U concentration in the solution is less than 100 ppb after blank correction were not considered for this study. Zircon ages were corrected for α-ejection (F_T) following Ketcham et al. (2011).

4. Results and interpretation

4.1. Thermometric and thermochronological data

Results of the RSCM are presented in Table 1 and Figs. 2 to 4 and show T_{max} ranging from 229 to 387 °C. In details, T_{max} ranges between 333 and 385 °C in the Chamonix syncline (Figs. 3, 4), between 265 and 301 °C in the North of the Aiguilles Rouges massif (Fig. 2), between 344 and 351 °C in the southern Aiguilles Rouges massif (Fig. 2), and between 229 and 320 °C in the cover West to the Aiguilles Rouges massif (with a clear NW–SE gradient) (Figs. 2, 4). Thus, above and around the Aiguilles Rouges massif, T_{max} is rather constant, about 320 °C with a +/− 25 °C dispersion (Figs. 3, 4A). East of the Mont Blanc massif, the T_{max} range is between 320 °C and 387 °C similar to the T_{max} range to the West of the massif (Figs. 3, 4A, B). Therefore, around the Mont Blanc massif, T_{max} is about 350 °C with a +/− 30 °C dispersion (Fig. 4A, B).

ZHe analyses are presented in Table 2 and associated ages are plotted on Figs. 2 to 5. Ages from the three sampling areas are quite similar: from 5.8 to 7.9 Ma for Brevent samples, 3.9 to 6.4 Ma for Prarion samples, and from 5.9 to 6.7 Ma for Pormenaz samples (Figs. 2, 3, 5). Prarion samples reveal ages increasing with elevation; Pormenaz samples also display a positive age/elevation relationship with a similar trend

Table 1
Raman spectroscopy of carbonaceous material data. The choice between the RA1 ratio of Lahfid et al. (2010) and the R2 ratio of Beyssac et al. (2002b) depends on best fit within Raman spectra. Spectra were post-processed using the software PeakFit following the methods described in Beyssac et al. (2002b) and Lahfid et al. (2010). (n) is the number of spectra used to calculate the mean ratio (RA1 or R2) and the standard deviation (sdv). The absolute error on temperature is ±50 °C for the Beyssac et al. (2002b) method and ±25 °C for the Lahfid et al. (2010) method.

	Latitude	Longitude	Unit	n	RA1/R2 Ratio	T(°C)	sdv (°C)	Method
MB11-43	45°55′46.6″	4°40′34.8″	Low.-mid. Ju.	12	0.62	**307**	9	Lahfid et al. (2010)
ALP14-23	45°55′23.3″	6°40′56.6″	Low.-mid. Ju.	13	0.62	**311**	19	Lahfid et al. (2010)
ALP14-24	45°55′23.3″	6°40′56.6″	Low.-mid. Ju.	13	0.63	**314**	6	Lahfid et al. (2010)
ALP14-26	45°55′23.3″	6°40′56.6″	Low.-mid. Ju.	12	0.63	**313**	8	Lahfid et al. (2010)
ALP14-28	45°57′24.5″	6°38′49.0″	Low.-mid. Ju.	12	0.61	**292**	6	Lahfid et al. (2010)
ALP14-29	45°57′24.5″	6°38′49.0″	Low.-mid. Ju.	12	0.6	**285**	9	Lahfid et al. (2010)
ALP14-33	45°59′23.8″	6°38′11.7″	Up. Ju.-Low.Cr.	13	0.56	**229**	8	Lahfid et al. (2010)
ALP14-35	45°54′19.7″	6°38′28.0″	Mid. Ju.	13	0.59	**268**	5	Lahfid et al. (2010)
ALP14-36	45°54′19.7″	6°38′28.0″	Mid. Ju.	14	0.63	**320**	5	Lahfid et al. (2010)
MB14-2	45°55′45.1″	6°43′08.8″	Low.-mid. Ju.	14	0.63	**317**	7	Lahfid et al. (2010)
MB14-7	45°56′41.2″	6°42′50.2″	Mid. Ju.	13	0.63	**315**	22	Lahfid et al. (2010)
ALP14-18	46°00′17.7″	6°56′42.8″	Up. Ju.	13	0.64	**333**	16	Lahfid et al. (2010)
ALP14-21	45°59′54.9″	6°56′47.9″	Low. Ju.	12	0.58	**385**	11	Beyssac et al. (2002b)
ALP14-02	45°51′50.0″	6°44′33.5″	Tr.	12	0.65	**349**	8	Lahfid et al. (2010)
ALP14-05	45°51′50.0″	6°44′33.5″	Tr.	13	0.64	**334**	19	Lahfid et al. (2010)
ALP14-06	45°52′12.3″	6°42′08.0″	Low. Ju.	13	0.66	**349**	14	Lahfid et al. (2010)
ALP14-07	45°52′12.3″	6°42′08.0″	Low. Ju.	12	0.66	**351**	9	Lahfid et al. (2010)
ALP14-07b	45°52′12.3″	6°42′08.0″	Low. Ju.	13	0.65	**344**	9	Lahfid et al. (2010)
MB14-21	45°52′19.4″	6°46′03.9″	Low. Ju.	15	0.67	**342**	3	Beyssac et al. (2002b)
MB14-23	45°52′36.1″	6°45′34.1″	Low. Ju.	10	0.67	**345**	4	Beyssac et al. (2002b)
MB14-47	45°50′48.9″	6°44′02.2″	Up. Car.	10	0.67	**343**	4	Beyssac et al. (2002b)
ALP14-08	46°10′47.6″	6°59′44.5″	Up. Ju.	13	0.61	**294**	6	Lahfid et al. (2010)
ALP14-10	46°10′93.6″	6°59′50.8″	Up. Ju.	15	0.61	**299**	10	Lahfid et al. (2010)
ALP14-11	46°11′09.8″	6°59′59.4″	Up. Ju.	16	0.59	**269**	7	Lahfid et al. (2010)
ALP14-12	46°11′09.5″	7°00′02.9″	Up. Ju.	12	0.62	**302**	16	Lahfid et al. (2010)
ALP14-14	46°11′09.5″	7°00′10.9″	Up. Ju.	16	0.61	**299**	6	Lahfid et al. (2010)
ALP14-15	46°11′09.4″	7°00′10.8″	Up. Ju.	12	0.61	**298**	10	Lahfid et al. (2010)
MB12-27	45°47′57.75″	6°56′21.30″	Low.-mid. Ju.	12	0.62	**366**	13	Beyssac et al. (2002b)
MB12-28	45°48′46.52″	6°57′06.61″	Low.-mid. Ju.	12	0.58	**387**	9	Beyssac et al. (2002b)
MB12-29	45°48′10.94″	6°57′42.84″	Low.-mid. Ju.	12	0.63	**321**	9	Lahfid et al. (2010)

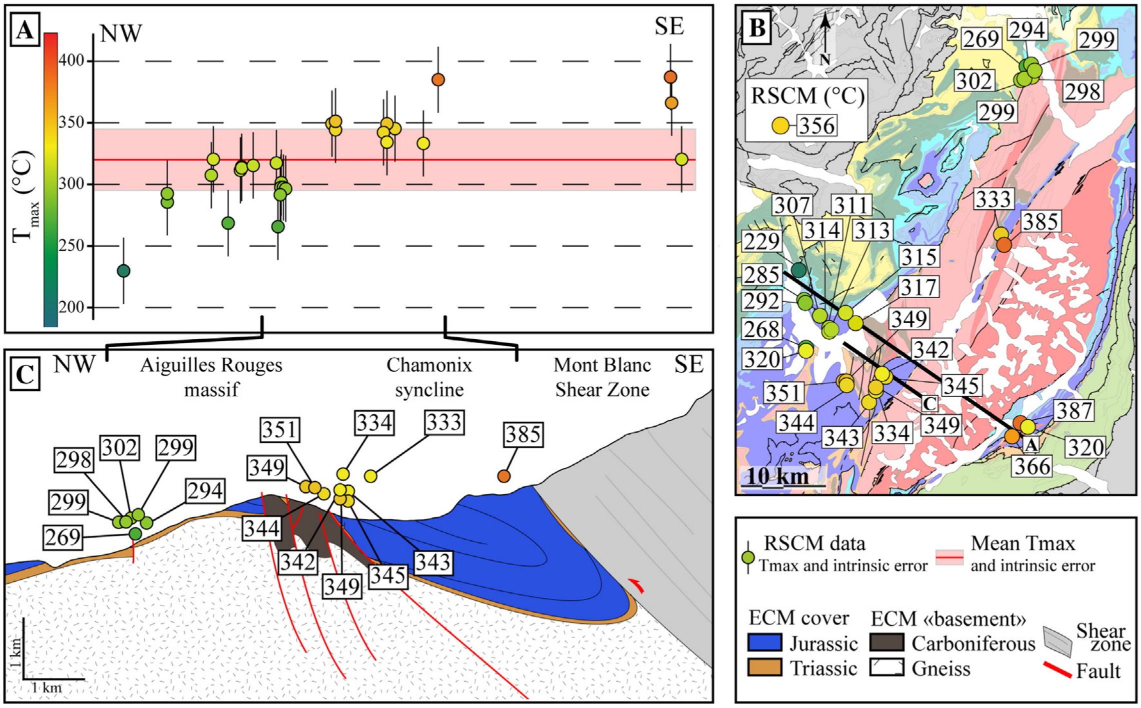

Fig. 4. Distribution of RSCM data. A. Temperature–distance distribution for all RSCM data on a NW–SE profile parallel to the cross section direction presented in Fig. 3. Maximal temperature slowly decreases from SE (385 °C) to NW (269 °C). The red line ($T = 320$ °C) corresponds to mean RSCM value in the Aiguilles Rouges cover and the pink field is the corresponding +/−25 °C data error (Lahfid et al., 2010). Maximal temperature data profile is localized in B. B. RSCM data map distribution and maximal temperatures. C. Part of cross-section presented in Fig. 3 with projected RSCM data. Cross section is localized in B. (For interpretation of the references to color in this figure legend, the reader is referred to the web version of this article.)

(Fig. 5A). The age/elevation relationship for the Brevent samples is not clear and suggests an unrealistic negative age/elevation relationship (Fig. 5A) with low-elevation samples older than high-elevation ones.

The three sampling profiles (Brevent, Prarion and Pormenaz, Fig. 2) show the following ranges for eU distribution: from less than 150 ppm to about 1180 ppm for Brevent, from 180 to 790 ppm for the Prarion, and from 190 to 1130 ppm for Pormenaz (Fig. 5B). ZHe ages are pretty constant over these eU ranges.

Except for two samples from Prarion, every sample yields a ZHe age similar or slightly older than the AFT ages given by samples located on the same area (Fig. 5B; Leloup et al., 2005; Seward and Mancktelow, 1994). The AHe samples from the North of the Aiguilles Rouges massif show an age distribution from 4.5 to 7.5 Ma (Valla et al., 2012), overlapping ZHe distribution ages (see Fig. 2 for location).

The ZHe data from the Mont Blanc massif were sampled at similar elevation, between 2000 and 2500 m (Fig. 5A). ZHe ages range between 5.8 and 9 Ma; eU varies from 240 and 780 ppm. This age–eU relationship is very similar to the one for the Aiguilles Rouges massif ZHe data (Fig. 5B).

4.2. Thermal modeling

These new ZHe data were combined with thermochronological data available in the literature in order to determine Temperature–time (T–t) paths for the Mont Blanc and the Aiguilles Rouges massifs. Thermal inversions were performed using the program HeFTy v.1.8.0 (Ketcham, 2005), which is based on the kinetic model of Guenthner et al. (2013) and He diffusion characteristics from Ketcham et al. (2011). In order to perform thermal inversions, of the Mont Blanc and the Aiguilles Rouges massif, we selected ZHe data from the same structural area (Fig. 6) and with similar elevations (Fig. 5). Then, we compute mean aliquot ages and eU for selected ZHe data and associate them to selected data from the literature as follow.

Most of literature data available for the Mont Blanc massif are located around the Mont Blanc tunnel (Fig. 2; Seward and Mancktelow, 1994; Leloup et al., 2005; Rolland et al., 2008; Glotzbach et al., 2008, 2011). Two of the ZHe ages were obtained in the Mont Blanc massif from samples close to the Mont Blanc tunnel (samples MBZ3 and MB12-19, elevation 2500–2600 m; Figs. 2 and 6) and were selected for the modeling of the Mont Blanc massif thermal history. As shown in Fig. 5B, ZHe ages are quite constant over the eU range. Therefore, we used mean age value for MBZ3 and MB12-19 ZHe data (Fig. 6), about 7.3 Ma (Fig. 5B) for the modeling of the Mont Blanc massif thermal history. In the Aiguilles Rouges massif, the data selected for thermal inversions were chosen because of their alignment along the NW continuation of the Mont Blanc tunnel (samples MBZ10 and MBZ14, elevation 2100–2500 m Figs. 2 and 6). As stated above, ZHe ages are quite constant over the eU range (Fig. 5B). We therefore used a mean age value of selected ZHe data, MBZ10 and MBZ14, about 6.4 Ma (Fig. 5B).

Moreover, as the distribution of eU values is the same for the two massifs (Fig. 5B), we determined a single mean eU value, about 529 ppm, that we associate with the mean ages calculated for both the Aiguilles Rouges and the Mont Blanc massifs. This ensures that, in HeFTy, we consider the same ZHe system closure temperature for both massifs.

Mean ZHe age/eU value determined for the Mont Blanc massif was combined in HeFTy with AFT, AHe and ZFT data from sample CGP22 located at an elevation of 2590 m, above the Mont Blanc tunnel (Fig. 6; Glotzbach et al., 2008, 2011). Mean age/eU value determined for the Aiguilles Rouges massif was combined in HeFTy with AFT data from sample ME131, located at an elevation of 2500 m (Figs. 5A, 6; Leloup et al., 2005). Note that AHe data available in the northern part of the Aiguilles Rouges massif (Valla et al., 2012) were impossible to combine with other thermochronological data because these ages are much older than AFT ages, which may be due to high eU content (see Valla et al., 2012). Therefore, those AHe data were not used in HeFTy thermal modeling.

Table 2
ZHe ages for samples from three Aiguilles Rouges profiles and for the Mont Blanc massif samples. See Fig. 2 for location. Ages are calculated following Ketcham et al. (2011). α-ejection (Ft) correction are calculated following Ketcham et al. (2011), and corrected from polishing following Reiners et al. (2007) considering an abrasion of 45 μm. e: excluded age.

		Sample	Latitude/ Longitude	Alliquote	Elevation (m)	Weight (mg)	Radius (μm)	^{4}He mes. ($*10^{-9}$ mol/g)	^{238}U calc. (ppm)	^{232}Th calc. (ppm)	^{147}Sm calc. (ppm)	eU (ppm)	Ft	Th/U	Measured age (Ma)	Corrected age (Ma)	+/− (Ma)	Mean corrected age (Ma)
Aiguilles Rouges massif	**Brevent**	MBZ6	45°54′54.58″N/	a	1024	0.009	63	12.8	387	70	2.2	403.78	0.85	0.18	5.9	6.9	0.4	6.9
			6°49′37.83″E	c	1024	0.013	70	30.2	954	192	5.7	999.67	0.86	0.20	5.7	6.4	0.4	
		MBZ7	45°54′54.58″ N /	b	1024	0.015	77	11.4	296	65	2.6	311.47	0.86	0.22	6.2	7.7	0.5	7.8
			6°49′37.83″ E	c	1024	0.014	76	6.1	150	30	0	157.97	0.87	0.20	6.6	8.2	0.5	
		MBZ8	45°55′6.18″ N /	b	1077	0.008	61	5.1	138	44	3.0	149.31	0.84	0.32	5.4	7.5	0.4	7.1
			6°51′7.07″ E	c	1077	0.011	66	7.2	237	35	8.5	245.28	0.86	0.15	5.0	6.3	0.4	
				d	1077	0.063	114	4.8	87	106	7.3	112.16	0.92	1.22	7.6	8.5	0.5	
				e	1077	0.029	89	14.7	477	59	5.1	491.78	0.90	0.12	5.4	6.2	0.4	
				f	1077	0.033	94	6.1	142	28	2.7	149.05	0.90	0.20	7.3	8.4	0.5	
		MBZ9	45°54′18.80″ N /	b	1336	0.019	85	19.0	490	84	4.0	510.32	0.88	0.17	6.8	7.8	0.5	7.2
			6°48′31.26″ E	c	1336	0.017	83	7.7	222	59	3.6	236.77	0.88	0.26	5.7	6.8	0.4	
		MBZ10	45°55′23,68″ N /	c	2180	0.011	67	19.0	618	300	2.3	689.63	0.86	0.49	5.2	6.2	0.4	6.2
			6°49′44.98″ E															
		MBZ11	45°54′57.92″ N /	b	1825	0.018	86	4.1	986	169	9.0	1025.94	0.88	0.17	0.7	0.8e	0.1	
			6°49′37.83″ E	c	1825	0.007	59	31.1	1130	242	11.6	1187.28	0.84	0.21	4.7	5.8	0.3	5.8
	Prarion	MBZ2	45°55′55.39″ N /	a	1039	0.050	112	18.5	714	20	2.1	719.51	0.92	0.03	4.7	5.2	0.3	5.3
			6°44′3.40″ E	b	1039	0.029	100	34.1	313	287	7.4	380.63	0.90	0.92	16.6	18.7e	1.1	
		MBZ4	45°53′21.33″ N /	a	1874	0.025	90	6.1	216	34	0.2	224.34	0.89	0.16	4.9	5.6	0.3	5.9
			6°45′13.08″ E	b	1874	0.026	90	8.6	282	42	4.4	292.04	0.89	0.15	5.4	6.1	0.4	
		MBZ5	45°52′22.23″ N /	a	1531	0.019	85.1	17.8	735	253	15.6	791.79	0.89	0.34	4.1	4.7	0.3	5.5
			6°44′20.33″ E	b	1531	0.018	99.2	5.6	176	27	4.5	187.67	0.90	0.15	5.6	6.4	0.4	
	Pormenaz	MBZ12	45°54′55.84″ N /	a	847	0.049	120	13.4	611	323	7.0	687.09	0.91	0.53	3.6	3.9	0.2	3.9
			6°46′14.41″ E															
		MBZ14	45°57′13.50″ N /	a	2111	0.025	87	9.7	268	225	11.9	321.37	0.89	0.84	5.5	6.3	0.4	6.5
			6°47′38,84″ E	b	2111	0.028	94	9.1	237	188	16.4	281.38	0.90	0.79	5.9	6.7	0.4	
		MBZ15	45°57′38.14″ N /	a	1853	0.055	121	18.1	466	367	18.8	552.85	0.92	0.79	6	6.6	0.4	6.7
			6°47′7.98″E	b	1853	0.044	115	13.5	1084	188	13.2	1128.91	0.91	0.17	2.2	2.5e	0.1	
		MBZ16	45°57′42.94″ N /	a	1702	0.054	110	32.8	939	464	60.1	1049.01	0.92	0.49	5.7	6.3	0.4	6.1
			6°46′59.91″ E	b	1702	0.031	103	21.4	667	349	18.5	749.01	0.90	0.52	5.1	5.9	0.3	
Mont Blanc massif		MBZ1	45°43′28.58″ N /	c	1955	0.005	52	76.6	950	212	14.1	1000.27	0.83	0.22	14.2	17.2e	1.0	e
			6°44′1.86″ E															
		MBZ3	45°5128.32″ N /	a	2591	0.006	61	20.5	625	21	7.9	630.14	0.84	0.03	6.0	7.2	0.4	8.1
			6°48′16.39″ E	b	2591	0.006	59	22.6	525	134	4.7	557.19	0.83	0.26	7.5	9.0	0.5	
		MBZ13	45°43′57.94″ N /	a	2390	0.015	78	8.2	286	62	4.0	300.71	0.87	0.22	5.1	5.8	0.3	7,0
			6°42′30.82″ E	b	2390	0.005	53	9.8	252	77	8.2	270.14	0.82	0.31	6.7	8.2	0.5	
		MB12–25	45°47′52.57″ N /	b	2130	0.004	48	13.4	437	153	5.3	473.56	0.81	0.35	5.2	6.4	0.4	6.4
			6°56′31.47″ E	c	2130	0.006	55	6.9	229	57	2.8	242.61	0.83	0.25	5.3	6.4	0.4	
		MB12–19	46°0′8.13″ N /	b	2509	0.013	73	17.6	391	228	65.3	444.69	0.87	0.58	7.3	8.4	0.5	7.3
			6°58′47.32″ E	c	2509	0.010	70	22.6	767	64	3.2	782.40	0.86	0.08	5.3	6.2	0.4	

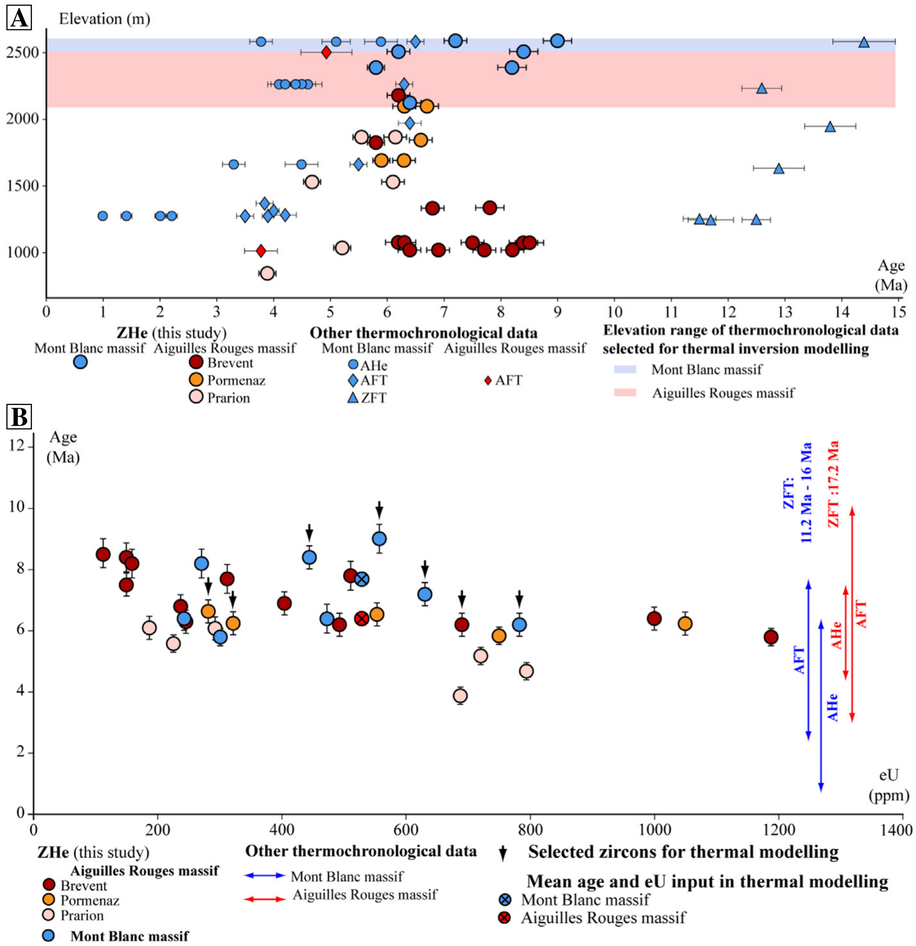

Fig. 5. A. Age/elevation distribution of the thermochronological data on the Aiguilles Rouges massifs (red dots) and on the Mont Blanc massif (blue dots) localized close to our ZHe samples. Aiguilles Rouges: AFT data from Rahn (1994) and (Leloup et al., 2005). Mont Blanc: ZFT, AFT and AHe data from Glotzbach et al. (2008, 2011) (see Fig. 2 for sample location). B. Age/eU distribution of the ZHe data from the Aiguilles Rouges massif (red dots) and from the Mont Blanc massif (blue dots). Double arrows are AHe, AFT and ZFT ages available on the Mont Blanc massif (in blue) and on the Aiguilles Rouges massif (in red) (Seward and Mancktelow, 1994; Rahn, 1994; Fügenschuh and Schmid, 2003; Leloup et al., 2005; Glotsbach et al., 2008, 2011; Valla et a., 2012). Two mean zircons (crossed circles), used in thermal modeling, are characterized by a mean eU value. This value is calculated from selected samples which are located close to the Mont Blanc tunnel and between 2100 and 2600 m. Those selected samples are MBZ10, MBZ14 for the Aiguilles Rouges massif and MBZ3, MB12–19 for the Mont Blanc massif (black arrows). See text for explanation. (For interpretation of the references to color in this figure legend, the reader is referred to the web version of this article.)

In HeFTy, the procedure consists in randomly testing 300,000 T–t paths for each model. T–t paths were statistically evaluated and categorized by their value of goodness of fit (GOF), calculated separately for the age data using the equation of Ketcham (2005). 'Acceptable' results (Fig. 7) correspond to a 0.05 GOF value whereas 'good' results correspond to 0.5 (See Ketcham, 2005). A mean T–t path is also plotted (Fig. 7).

Inverted thermal models for the Aiguilles Rouges massif are presented in Fig. 7A and B. In Fig. 7B, thermal inversion is further constrained by ZFT data from Soom (1990) with a constraint box characterized by a few Myrs duration (range of ZFT data from Soom (1990), 15.5–18.9 Ma) and a large temperature range (220–300 °C, closure temperature of ZFT system; e.g., Rahn et al., 2004; Garver et al., 2005; Bernet, 2009). Maximal temperature reached by the AR massif is constrained by mean temperature from RSCM analysis on the Aiguilles Rouges massif cover rocks (320 +/− 25 °C, see discussion for RSCM data interpretation). The oldest age for the T_{max} in the Aiguilles Rouges massif is constrained by the age of the youngest sedimentary rocks deposited above the massif (Val d'Illiez sandstone formation, 32–29 Ma, Sinclair, 1997). The youngest age is constrained by both the activation around 18 Ma of the thrusts in the North Alpine Foreland Basin, which are connected to crustal ramps underneath the Aiguilles Rouges massif (Burkhard and Sommaruga, 1998) and the cooling initiation of the Morcles nappe at 15–17 Ma (Kirschner et al., 1995). Finally, Aiguilles Rouges massif thermal modeling (Fig. 7A and B) indicates that, whatever it is constrained by ZFT data (Fig. 7A) or not (Fig. 7B), cooling of the massif initiated around 18 +/−1 Ma with a rather constant cooling rate, about 5–10 °C Ma^{-1} from 16 Ma until 8 Ma (Fig. 7A, B). A higher cooling rate is suggested between 16 and 18 Ma (Fig. 7A), around 15–20 °CMa^{-1}. However, this cooling rate is supported only by one data and thus should be considered with care. Around 8 Ma, the cooling rate increased to 20–25 °C Ma^{-1} (Fig. 7A, B). Because AHe data available in the northern part of the massif (Valla et al., 2012) could not be inverted with our dataset in HeFTy software, cooling path of the Aiguilles Rouges massif between 3 Ma and present remains speculative and is represented as similar to the Mont Blanc massif one (see below, Fig. 8).

The inverted thermal history of the Mont Blanc massif (Fig. 7C) is also constrained by ZFT data from Glotzbach et al. (2010) (sample CGP22, Fig. 6). ZFT constraint box is characterized by a few Myrs duration (range of ZFT data from Glotzbach et al. (2010), 13.3–15.5 Ma) and a large temperature range (220–300 °C, closure temperature of ZFT system, e.g., Rahn et al., 2004; Garver et al., 2005; Bernet, 2009). Peak temperature is constrained from multiequilibrium analysis of syn-kinematic phases from alpine shear zones (400 +/− 25 °C, Rolland et al., 2003). The initiation of cooling is constrained by the youngest syn-kinematic phengites, dated by geochronological

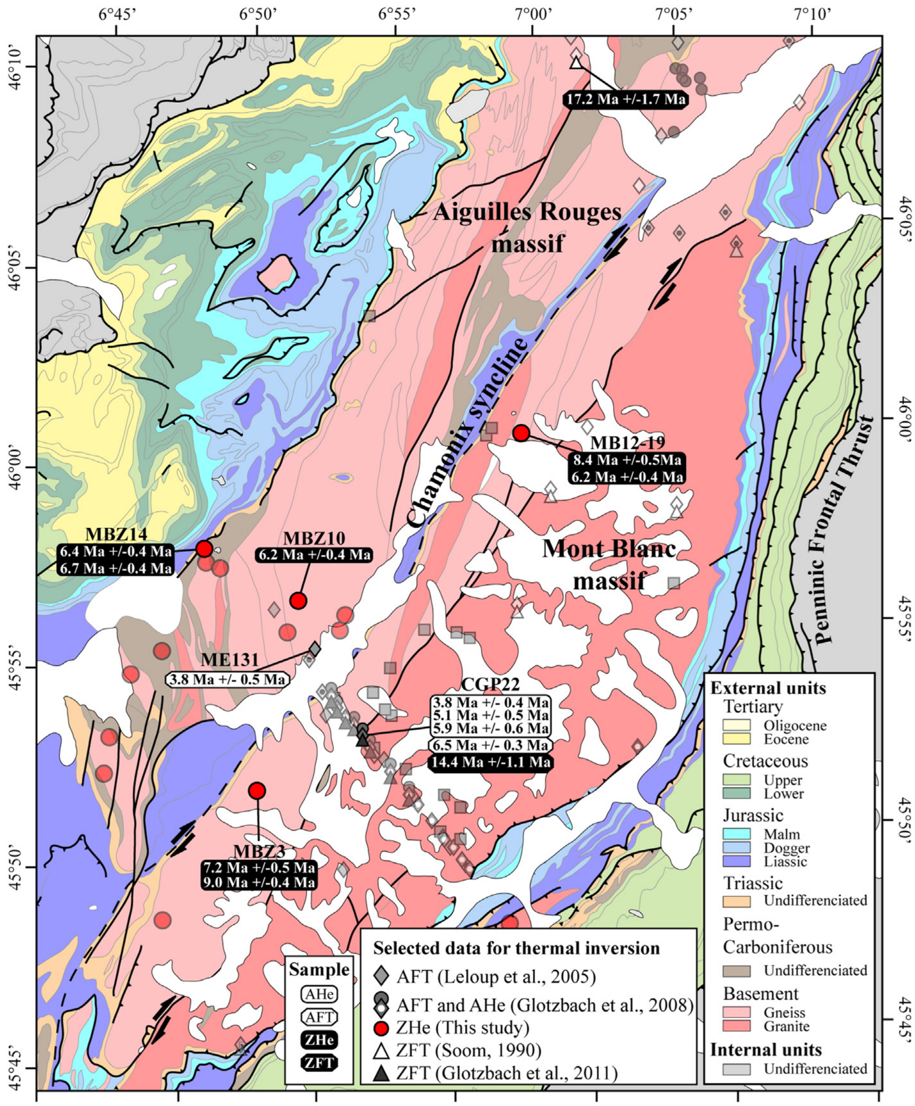

Fig. 6. Geological map with data selected for the thermal inversion with HeFTy software. All selected samples are close to the Mont Blanc tunnel and at similar elevation. In the Mont Blanc massif, the selected samples are in the Mont Blanc Shear Zone at elevation of 2500–2600 m (MBZ3 and MB12-19). In the Aiguilles Rouges massif, the selected samples are along a section corresponding to the NW continuation of the Mont Blanc tunnel at elevation about 2100–2500 m (MBZ10, MBZ14). Note the exception of the ZFT sample from Soom (1990), which is in the NE part of the Aiguilles Rouges massif.

^{40}Ar/^{39}Ar data (Rolland et al., 2008). Cooling initiated around 16–20 Ma with a cooling rate around 30–35 °C Ma^{-1} until about 14 Ma, before slowing down at 10–15 °C Ma^{-1} from 14 to 8 Ma. Around 8 Ma, cooling rate strongly increased to 40–45 °C Ma^{-1} until 5–6 Ma before slowing down to 5–10 °C Ma^{-1}.

4.3. Interpreted thermal histories

Fig. 8, displays complete thermal paths for the Mont Blanc and the Aiguilles Rouges massifs interpreted from thermal inversions for the cooling phase and from the literature for the earlier phases. For the Mont Blanc massif, the cooling part of the thermal path has been redrawn following mean T–t path obtained in HeFTy software (Fig. 7C). Initiation of cooling is poorly constrained in HeFTy thermal inversion by a Time-temperature box (^{40}Ar/^{39}Ar dating of syn-kinematic phengite and thermobarometric analysis of syn-kinematic phases into alpine shear zone). Therefore, the thermal path of the Mont Blanc massif is simply redrawn through the center of the HeFTy constraint box (18 Ma, 400 °C).

For the Aiguilles Rouges massif, the cooling part of the thermal path has been redrawn following the mean T–t path from HeFTy (Fig. 7A) in order to take into account ZFT data from Soom (1990). The end of the thermal peak of the Aiguilles Rouges massif (320 +/−25 °C) was probably coeval with the age of activation of the Subalpine Molasse thrust connected to crustal ramps beneath the Aiguilles Rouges massif, i.e., at about 17–19 Ma (Burkhard and Sommaruga, 1998). This would imply a variation in the cooling rate at about 16 Ma (Fig. 8), but the thermal path between 16 and 20 Ma remains poorly constrained. Finally, the end of the cooling history (between 3 and 0 Ma) is also poorly constrained. Thus, the thermal path during this time interval was tentatively drawn as the Mont Blanc one.

5. Discussion

5.1. Thermal peak and thermal structure

Around the Aiguilles Rouges (AR) massif, the RSCM maximum temperatures obtained on samples from metasedimentary rocks range

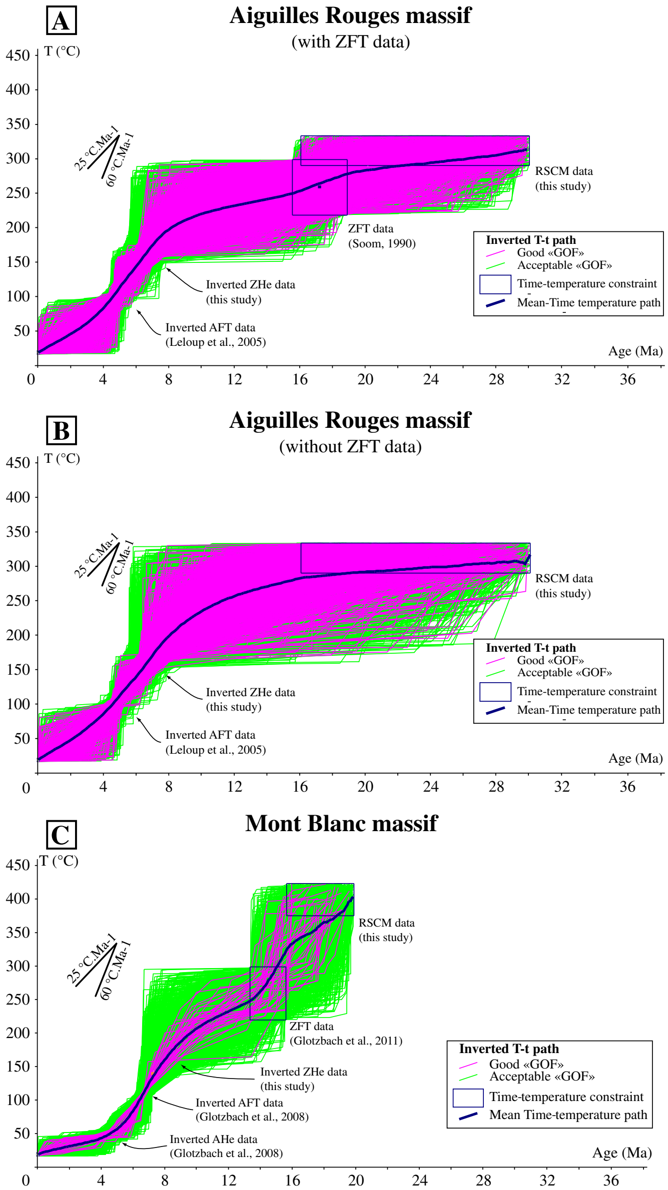

Fig. 7. Thermal histories modeled with HeFTy software. T–t paths are statistically evaluated and categorized by their value of goodness of fit (GOF). 'Acceptable' results, in green, correspond to a 0.05 GOF value and 'good' results, in purple, correspond to 0.5 GOF (Ketcham, 2005). A, B. Thermal history modeling for the Aiguilles Rouges massif. Inverted data are ZHe (see Fig. 5 for eU and age calculations) and AFT (sample ME131, Leloup et al., 2005). Inversion is also constrained by T_{max} reached by the autochtonous cover of the massif (320 °C +/− 25 °C, RSCM data, this study, see text for explanation). C. Thermal history modeling for the Mont Blanc massif. Inverted data are ZHe (see Fig. 5 for eU and age calculations), AFT and AHe data (CGP22 samples, Glotzbach et al., 2008). Thermal peak is constrained by multi-equilibrium analysis realized on syn-kinematic phases (Rolland et al., 2003) and dated by $^{40}Ar/^{39}Ar$ geochronology on syn-kinematic phengite (Rolland et al., 2008). In B and C, thermal inversions are also constrained by a ZFT data (14.4 Ma +/− 1.1 Ma, sample CGP22) from Glotzbach et al. (2010) and by ZFT data (17.2 Ma +/− 1.7 Ma) from Soom (1990), respectively. ZFT data are symbolized by a box defined by ZFT closure temperatures about 220–300 °C (e.g., Rahn et al., 2004; Garver et al., 2005; Bernet, 2009) and age range. (For interpretation of the references to color in this figure legend, the reader is referred to the web version of this article.)

between 265 °C and 351 °C and most fall close to 320 +/− 25 °C (red area, Fig. 4A). These metasedimentary rocks most likely represent the former cover of the AR massif (Escher et al., 1993; Escher and Beaumont, 1997). North of the massif (in Switzerland), the cover is not detached from the basement (Fig. 2, Ayrton et al., 1987). Even though a décollement is mapped in the southern part (Fig. 2, Leloup et al., 2005), we can safely consider that the displacement remained limited for the sake of along-strike structural consistency. Therefore, the T_{max} of 320 +/− 25 °C recorded in the cover rocks of the AR massif likely represents a lower bound for the T_{max} of the underlying basement.

In the Morcles nappe, i.e., the cover of the Mont Blanc (MB) massif currently located above the AR massif, oxygen isotopic fractionation data between quartz and calcite in textural equilibrium in veins provided temperatures about 350 +/− 30 °C (Fig. 8, Kirschner et al., 1995). This result is consistent with our RSCM data obtained in the Chamonix basin, located between the AR and the MB massifs, and east of the MB massif, at about 350 +/− 25 °C (Fig. 4). Thus, the thermal peak reached by the cover of the MB massif is consistent with the thermal peak of 400 +/− 25 °C determined in Alpine basement shear zones (Rolland et al., 2003) (Fig. 8).

Moreover, in the cover of both the MB and AR massifs, peak temperatures are quite similar (350 °C and 320 °C, respectively with a +/− 30 °C maximum dispersion) over 20–30 km from NW to SE (Figs. 2 and 4). Similar results were obtained in the Oisans massif further South, where RSCM peak temperatures for cover rocks are around 330 +/− 25 °C (Fig. 8), constant over a distance of 75 km (Bellanger et al., 2015).

5.2. Thermal peak duration and coeval shortening

In the MB massif, the onset of activation of the Alpine shear zones shortly post-dated the last sediments, the Tavayennaz sandstone formation, which was deposited above the massif between 32 and 34 Ma (Sinclair, 1997). Close to the Mont Blanc tunnel, P–T conditions and ages of deformation within several Alpine shear zones are available in the literature: thermobarometric data on syn-kinematic phases indicate equilibrium conditions at about 400 °C (Rolland et al., 2003; Rossi et al., 2005) and the corresponding syn-kinematic minerals were dated between 30 and 14 Ma (Rolland et al., 2008; Cenki-Tok et al., 2013; Egli et al., 2015). In veins, the P–T conditions of post-kinematic fluid circulations (14–11 Ma, Rossi and Rolland, 2014) were estimated from quartz fluid inclusions and chlorite thermometry at 300–350 °C and 2.5–3 kbar (Poty et al., 1974; Fabre et al., 2002; Rossi et al., 2005). Therefore, syn-kinematic mineral phases may have crystallized in shear zones from 30 Ma until 14 Ma under a relatively constant temperature of about 400 °C. Moreover, Glotzbach et al. (2011) obtained ZFT ages at about 14–15 Ma from samples in the central part of the Mont Blanc massif. This ZFT age indicates that the MB massif cooling initiated before 14 Ma. The MB massif therefore likely experienced a 10–15 Myrs long thermal peak at about 400 °C (Fig. 8).

The youngest sedimentary rocks deposited above the Morcles nappe are dated at 29–31 Ma (Ruffini et al., 1993) and Kirschner et al. (2003) suggested a rapid burial and heating for the nappe. The Diableret thrust, located just above the Morcles nappe, accommodated most of its displacement early in its history around 28–30 Ma (Kirschner et al., 2003). In the normal limb of the Morcles nappe, syn-kinematic veins formed at 250 °C to 285 °C (Kirschner et al., 1995). In the highly-sheared reverse limb of the nappe, syn-kinematic veins were continuously formed close to the peak temperature, whatever the vein generation, between 300 and 350 °C (Kirschner et al., 1995). Within the nappe, Burkhard and Goy-Eggenberger (2001) showed that isotherms for anchizone (200 °C) and epizone (300 °C) are less folded than the meta-sedimentary layers and dip toward the NW. Moreover, syn-kinematic phengites sampled in the sheared reverse limb of the nappe were dated between 30 and 15 Ma (Kirschner et al., 1995, 2003). All those results suggest that the nappe was deformed during its thermal peak, between 30–27 Ma and 15 Ma, before its exhumation and extrusion from its former basin (Fig. 9A, B). Extrusion may have slowly initiated at 23 Ma with the initiation of the MBSZ, though temperature was similar until 16–18 Ma (Fig. 9C, D). After this time period, cooling of the massif including the MBSZ may have been passive (Fig. 9E, F, G) as no or few ages of deformation are found in the MBSZ. Finally, this thermal history is consistent with the last

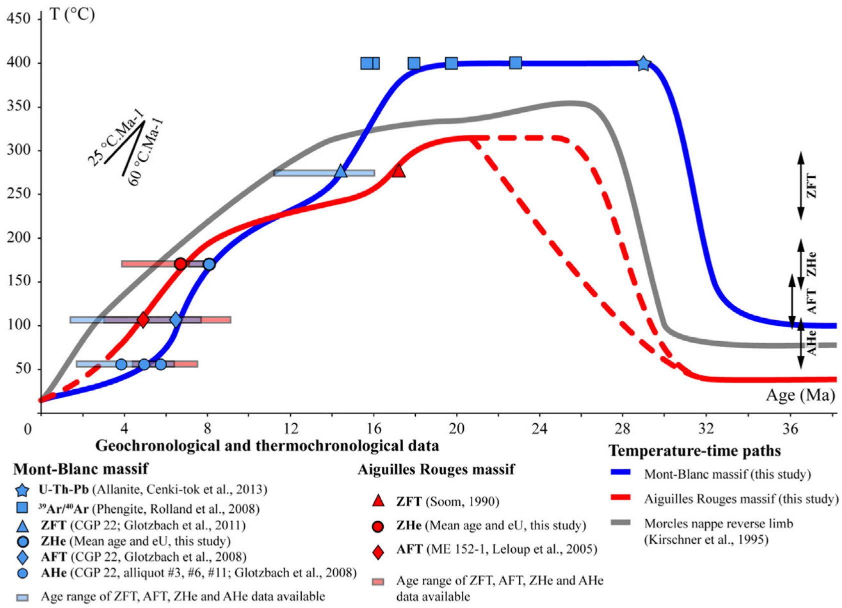

Fig. 8. Complete temperature–time paths for the Mont-Blanc and Aiguilles Rouges massifs from our thermal modeling and geological constraints. Closure temperatures reported on the figure as double black arrows are: 300–220 °C for ZFT (e.g., Rahn et al., 2004; Garver et al., 2005; Bernet, 2009), 140–195 °C for ZHe (Reiners et al., 2002; Stockli, 2005, Guenthner et al., 2013), 95–160 °C for AFT (Gallagher et al., 1998), and 50–110 °C for AHe (Farley, 2000; Shuster and Farley, 2009). The onset of the burial, and heating, of the Mont Blanc and Aiguilles Rouges massifs is estimated from the deposition of Tavayennaz (36–32 Ma) and Val d'Illez (32–29 Ma) formations, respectively (Sinclair, 1997). Temperature peak in the Mont Blanc massif is estimated at 400 +/− 25 °C from thermobarometric analysis of syn-kinematic phases in alpine shear zones (Rolland et al., 2003; Rossi et al., 2005). The Aiguilles Rouges maximal burial temperature is determined from new RSCM data (320 +/− 25 °C). Cooling of both massifs is drawn following mean T–t paths modeled with HeFTy software. End of thermal peak and initiation of cooling is constrained for the Mont Blanc massif by the last ages of syn-kinematic phengite crystallization under maximum P–T condition ($^{40}Ar/^{39}Ar$ dating, Rolland et al., 2008; multi-equilibrium analysis of syn-kinematic phases, Rolland et al., 2003). End of thermal peak and initiation of cooling is constrained in the Aiguilles Rouge massif by the activation of the Subalpine Molasse Thrust at 17–19 Ma, which is connected to crustal ramps localized beneath the AR massif (Burkhard and Sommaruga, 1998).

evidence of the major Helvetic thrust activity, slightly reactivated between 25 and 15 Ma and inactive after 15 Ma (Crespo-Blanc et al., 1995; Kirschner et al., 2003). Additionally, considering a 30 °C error on the thermometer used to define the crystallization temperature of the syn-kinematic vein minerals of the Morcles nappe reverse limb (Sharp and Kirschner, 1994; Kirschner et al., 1995), we can define a thermal peak close to 350 °C (Fig. 8), which remained almost constant between 27 and 15 Ma. It appears that the thermal history of the Morcles nappe is quite similar to the MB one (Fig. 8), which is consistent with the structural interpretation of synchronous deformation between the MB massif and the Morcles nappe, the latter being the cover of the former.

The MB shear zones (30–14 Ma, see above) were active during the thermal peak and therefore, this massif was shortened without any significant synchronous cooling (Fig. 8). Even the main shear zone of the MB massif, the Mont Blanc Shear Zone, which was active at least since 23 Ma (Rolland et al., 2008), did not significantly exhume and cool down the massif until 17 Ma to 19 Ma (Fig. 7).

In the northeastern part of the AR massif, Vernon et al. (2008) show that ZFT data were only partially reset and that they give ages inconsistent with the alpine collisional history. However, one ZFT data shows complete resetting (17.2 Ma; Soom, 1990; Vernon et al., 2008). This partial resetting of most ZFT ages in the AR massif is consistent with the peak temperature reached by the massif, about 310–320 °C (RSCM data, this study), i.e., just above the ZFT system annealing temperature (220–300 °C, e.g., Rahn et al., 2004; Garver et al., 2005; Bernet, 2009). In any case, the AR massif probably started cooling at 18 Ma +/− 1 Ma (Fig. 8). The youngest sedimentary rocks deposited above the AR massif, the Val d'Illiez sandstone formation, are Oligocene in age (32–29 Ma, Sinclair, 1997). Thus, two hypotheses can be made for the thermal history of the AR massif: (1) either it underwent slow heating (30 °C Ma^{-1}) between 32 and 20 Ma and immediately began to cool at 18 +/− 1 Ma (Fig. 8) or (2) the AR massif underwent a fast heating rate (60 °C Ma^{-1}) and experienced a long thermal peak (5–6 Myrs) (Fig. 8). From the comparison between the two T–t paths presented in Fig. 8, the scenario (2) appears to be the most realistic. Indeed, the three units (i.e. the Aiguilles Rouges massif, the Mont Blanc massif and the Morcles nappe) can be restored in a similar structural position (Burkhard and Sommaruga, 1998) and thus should have recorded nearly similar thermal histories.

Thus, following the continental subduction and exhumation of internal units, the initiation of the Alpine collisional phase was characterized by underthrusting of the ECM below the internal units (Fig. 9A). During this burial, the innermost Helvetic nappes (Diableret and Wildhorn nappes) were detached from their basement and stacked onto the Mont Blanc cover (future Morcles nappes; Fig. 9B). At the thermal peak, shortening occurred in the MB massif and Morcles nappe (Fig. 9C, D).

A several Myrs long thermal peak was also documented in other ECM along strike. In the Oisans massif, a peak temperature of 330 +/− 25 °C was reached at 33 Ma and remained constant until 25 Ma (Bellanger et al., 2015), as for the Argentera-Mercantour massif (Sanchez et al., 2011). Further North, in the Aar massif, Challandes et al. (2008) proposed, from 1D thermal modeling, that temperature increased at around 40 °C My^{-1} from 33 to 25 Ma, before reaching a quite constant temperature during 5–10 Myrs.

5.3. Cooling and exhumation

As shown before, cooling initiated around 18 Ma +/− 1 Ma in the AR massif. According to our ZHe results and AFT data from Leloup et al. (2005), inverted together with HeFTy software and combined with only one ZFT age (Soom, 1990) and with RSCM peak temperature constraints (Fig. 7A, B), the cooling rate of the AR massif is quite constant from 16 Ma to 8 Ma, about 5–15 °C Ma^{-1} (Fig. 8).

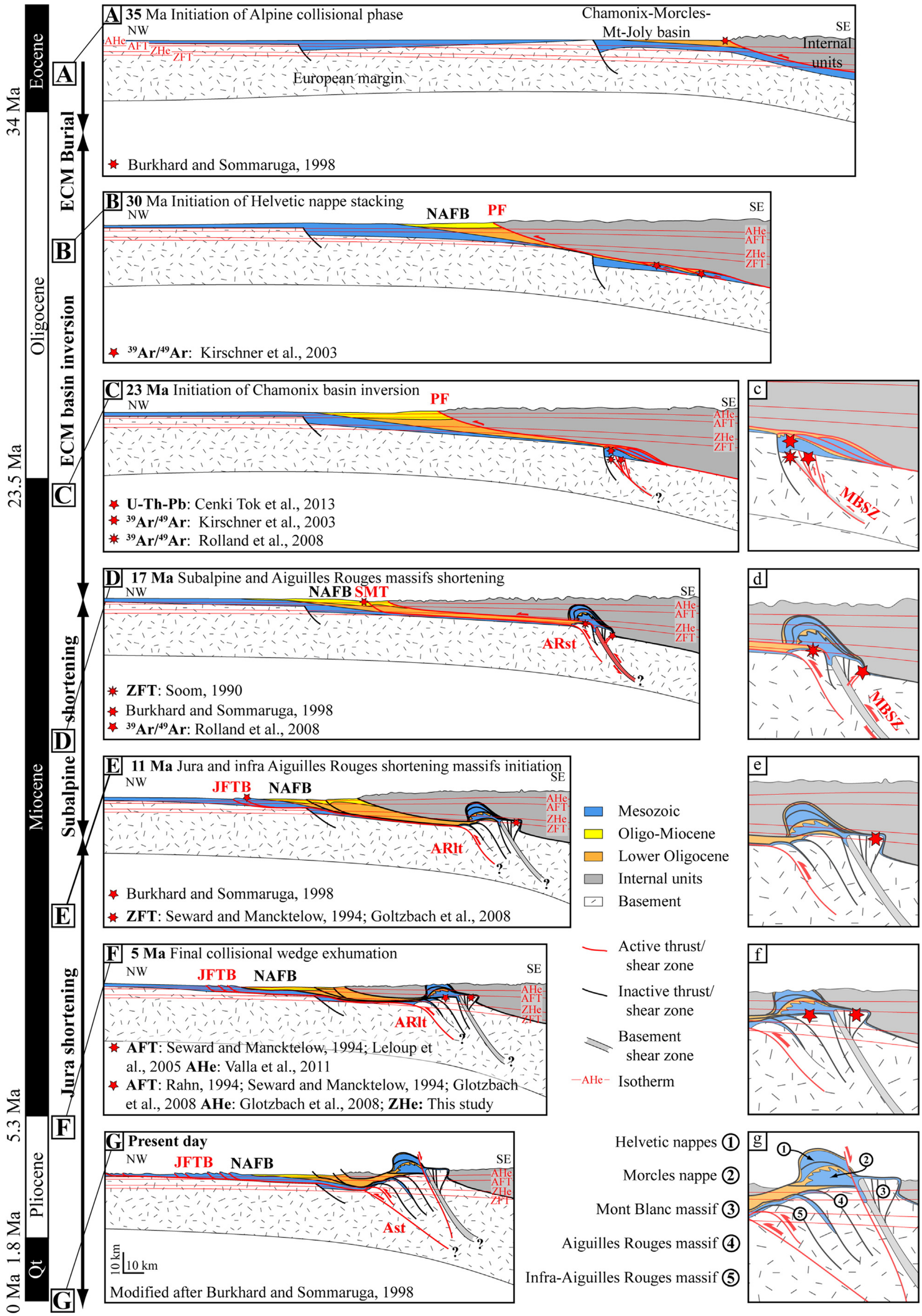

0 Ma
1.8 Ma
5.3 Ma
23.5 Ma
34 Ma
Qt
Pliocene
Miocene
Oligocene
Eocene
ECM Burial
ECM basin inversion
Subalpine shortening
Jura shortening
A 35 Ma Initiation of Alpine collisional phase
Chamonix-Morcles-Mt-Joly basin
NW
SE
Internal units
European margin
Burkhard and Sommaruga, 1998
B 30 Ma Initiation of Helvetic nappe stacking
NAFB
PF
39Ar/49Ar: Kirschner et al., 2003
C 23 Ma Initiation of Chamonix basin inversion
MBSZ
U-Th-Pb: Cenki Tok et al., 2013
39Ar/49Ar: Kirschner et al., 2003
39Ar/49Ar: Rolland et al., 2008
D 17 Ma Subalpine and Aiguilles Rouges massifs shortening
SMT
ARst
ZFT: Soom, 1990
Burkhard and Sommaruga, 1998
39Ar/49Ar: Rolland et al., 2008
E 11 Ma Jura and infra Aiguilles Rouges shortening massifs initiation
JFTB
ARlt
Burkhard and Sommaruga, 1998
ZFT: Seward and Mancktelow, 1994; Goltzbach et al., 2008
Mesozoic
Oligo-Miocene
Lower Oligocene
Internal units
Basement
Active thrust/ shear zone
Inactive thrust/ shear zone
Basement shear zone
AHe
Isotherm
F 5 Ma Final collisional wedge exhumation
AFT: Seward and Mancktelow, 1994; Leloup et al., 2005 AHe: Valla et al., 2011
AFT: Rahn, 1994; Seward and Mancktelow, 1994; Glotzbach et al., 2008 AHe: Glotzbach et al., 2008; ZHe: This study
G Present day
Ast
10 km
Modified after Burkhard and Sommaruga, 1998
Helvetic nappes 1
Morcles nappe 2
Mont Blanc massif 3
Aiguilles Rouges massif 4
Infra-Aiguilles Rouges massif 5

For the Mont Blanc massif, AHe, AFT and ZHe data (Leloup et al., 2005; Glotzbach et al., 2008; this study) were inverted with HeFTy software and combined with ZFT data (Seward and Mancktelow, 1994), $^{40}Ar/^{39}Ar$ geochronological data (Rolland et al., 2008) and thermobarometric data (Rolland et al., 2003) (Fig. 7C). T–t paths suggest the initiation of cooling of the MB massif between 16 and 19 Ma. Cooling rate of the MB massif was about 30–35 °C Ma^{-1} between 18 and 14 Ma and slowed down to 10–15 °C Ma^{-1} from 14 Ma until 8 Ma (Fig. 8).

For the Morcles nappe, cooling initiated around 15 Ma and its rate remained rather constant, at 25 °C Ma^{-1}, until 3 Ma (Kirschner et al., 1995). This cooling rate is quite similar to the AR massif and the MB ones, which is consistent with the structural interpretation that the Morcles nappe is the former cover of the MB massif (e.g., Escher et al., 1993; Burkhard and Sommaruga, 1998). Due to the activity of the Mont Blanc Shear Zone, the Morcles nappe was extruded from its former syn-rift basin (Chamonix inverted basin) during its temperature peak and then emplaced above the AR massif at around 15 Ma.

Just after the initiation of cooling, at 18 Ma +/− 1 Ma, the MB massif cooling rate was significantly higher than for the AR massif (30–35 °C Ma^{-1} and 15–20 °C Ma^{-1} respectively, Fig. 8). This difference of cooling rate from 18 to 14 Ma cannot be explained by the activity of crustal ramps located beneath both massifs, as such process would have implied the same cooling rate. Therefore, the higher cooling rate of the Mont Blanc massif could be explained by the activity of the MBSZ until 14 Ma, as proposed by Leloup et al. (2005) and Rolland et al. (2008). Both the frontal crustal ramp and the MBSZ may have been active between 18 and 14 Ma, allowing a faster cooling of the MB massif than the AR massif. After 14 Ma, the MBSZ stopped and remained inactive (Egli and Mancktelow, 2013) then both AR and MB massifs cooled at quite similar rates, about 5–15 °C Ma^{-1}, during a few Myrs (Fig. 8).

In our sequence of the Alpine collisional shortening and exhumation of the external zone (Fig. 9), the thermal peak ended at around 18 Ma. Both the Mont Blanc and the Aiguilles Rouges massifs were exhumed above frontal crustal ramps (Fig. 9D). At the end of thermal peak and at the onset of MB massif cooling, the Morcles nappe was extruded from the Chamonix basin, most likely due to the MBSZ activity. This extrusion is also suggested by the activation of a few shear zones at 16 Ma at the top of the Aiguilles Rouges massif ($^{40}Ar/^{39}Ar$ dating, Egli, 2013) and by the last deformations occurring in the Morcles nappe (Fig. 9D; Kirschner et al., 2003). Moreover, at about 16–18 Ma, the front of the collisional wedge propagated westward (Burkhard and Sommaruga, 1998). At this time, the MBBT was also active (Rolland et al., 2007, 2008; Fig. 9D). Thus, the crustal volume accreted by underplating significantly increased at this time. At 11 Ma, the Jura fold-and-thrust-belt started to form (Becker, 2000), linked to the initiation of basement ramps in the Infra Aiguilles Rouges massif (Fig. 9E; Burkhard and Sommaruga, 1998). Thus, throughout the collisional phase, the successive activation of the main thrusts/shear zones in these massifs indicates a forward sequence, except for the MBBT.

Around 8 Ma, in both the AR and the MB massifs, the cooling rates increased from 5–15 °C Ma^{-1} to 20–45 °C Ma^{-1}. Thus, it appears that the increase in cooling rates initially dated back to 5–6 Ma (Glotzbach et al., 2011 and references therein) may have been slightly older (around 8 Ma). Then, around 4–5 Ma, the cooling rate strongly decreased in the Mont Blanc massif, as already pointed out by Glotzbach et al. (2011), and was linked to a change in the exhumation rate. This change could be linked to either the decreasing rate of Alpine convergence (Schmid et al., 1996) and/or climate change and therefore the decrease of erosional efficiency (e.g., Whipple and Mead, 2006). Erosional efficiency drop could also be linked to the progressive exposure of the MB and the AR crystalline basement rocks after the erosion of their metasedimentary cover (Glotzbach et al., 2011). Yet, because AHe data available in the northern part of the AR massif could not be inverted, the late AR cooling history remains speculative and is not further discussed.

Further Northeast, in the Aar massif, the timing of exhumation/cooling is seemingly very similar to the *AR*-MB one. The main shearing event in the Aar massif is dated between 22 Ma and 20 Ma (Challandes et al., 2008; Rolland et al., 2009), while the cooling phase initiated at 17 Ma. Thus, the main shear zone activity is not coeval with any cooling of the massif. Northwest of the Aar massif, in the molasse basin, fold-and-thrust-belt structures initiated at 16–20 Ma and are connected to frontal ramps below the Aar massif (Burkhard, 1988). Thus, the Aar massif was internally shortened mainly during its thermal peak, then exhumed and cooled down due to the activity of frontal crustal ramp.

Similarly, further South, in the Oisans massif, shortening was accommodated in the basement by distributed shear zones dated between 32 and 25 Ma, coeval with the thermal peak (Simon-Labric et al., 2009; Bellanger et al., 2015) while cooling of the massif initiated at 25 Ma (Crouzet et al., 2001; van der Beek et al., 2010). Thus, as for the Mont Blanc-Aiguilles Rouges and the Aar massifs, cooling was not related to the activity of the distributed shear zones and the related internal shortening of the massif mainly occurred during the thermal peak.

From the comparison of the thermal evolution and the shortening sequence of the ECM along the Alpine arc, it appears that the typical evolution of the Alpine collisional wedge may be the following. After its underthrusting and burial below the internal (Penninic) units, the crust of the European margin underwent a two-stage evolution: it was shortened at its thermal peak during 5 to 10 Myrs, and subsequently exhumed and cooled down thanks to the activation of crustal ramps that propagated deformation in-sequence to the front of the collisional wedge, within the fold-and-thrust belts.

6. Conclusions

In this contribution, we report new RSCM data and (U–Th–Sm)/He thermochronological data on zircons (ZHe) obtained on samples from the basement of the Aiguilles Rouges and the Mont Blanc massifs and their metasedimentary cover. RSCM data show that the temperature peak reached by the Aiguilles Rouges cover was about 320 °C. Published data suggest that the temperature peak for the Mont Blanc massif, at 400 °C, was about 10–15 Myrs long. It is likely that the temperature peak of the Aiguilles Rouges massif was also quite long (5–10 Myrs). During these long thermal peaks, the major structure of the Mont Blanc massif, the Mont Blanc Shear Zone, was active but did not exhume

Fig. 9. Shortening sequence of the European proximal margin during the collisional Alpine phase. PF: Penninic Front; NAFB: North Alpine Foreland Basin; SMT: Subalpine Molasse Thrust; MBSZ: Mont Blanc Shear Zone; ARut Aiguilles Rouges upper thrust; ARlt: Aiguilles Rouges lower thrust; JFTB: Jura Fold and Thrust Belt. Closure temperature isotherms are: ZFT 300–220 °C (e.g. Rahn et al., 2004; Garver et al., 2005; Bernet, 2009); ZHe: 140–195 °C (Reiners et al., 2002; Stockli, 2005; Guenthner et al., 2013); AFT: 95–160 °C (Gallagher et al., 1998); AHe: 50–110 °C (Farley, 2000; Shuster and Farley, 2009). The thermal evolution is documented mainly along a NW–SE section, parallel to the Alpine shortening (Fig. 9). We assume that out of plane movements, in particular linked to the Rhône–Simplon transpressive dextral fault system, do not significantly modify the collisional wedge thermal structure in the area of the Mont Blanc/Aiguilles Rouges massifs. A. End of continental subduction of the distal European margin and initiation of underthrusting of the proximal European margin below the internal (Penninic) units. B. Stacking of the Helvetic nappes (Diableret and Wildhorn) above the future Morcles nappe. C. First deformations within the Morcles nappes linked to the initiation of shortening within the Mont Blanc massif at 29.5 Ma. The Mont Blanc shear zone is activated at the end of this stage at 23 Ma. D. Initiation of the crustal ramps below the Aiguilles Rouges massif and activation of the Mont-Blanc Back-Thrust (MBBT). E. Westward propagation of crustal deformation as suggested by the activation of the Jura décollement connected to the deformation of the infra Aiguilles Rouges massif. F. Progressive exhumation of both the Aiguilles Rouges and Mont-Blanc massifs. H. Present-day stage (modified after Burkhard and Sommaruga, 1998) with the Simplon transtensional fault.

significantly the crust. Similar results were already obtained in other ECM such as the Oisans massif.

Thermal modeling of our thermochronological data coupled to published data suggests that cooling initiated in the Mont Blanc massif at around 18 Ma +/− 1 Ma. The Miocene cooling rate, in the Mont Blanc massif, was about at 30–35 °C Ma^{-1} between 18 and 14 Ma and slowed down to 10–15 °C Ma^{-1} at 14 Ma and until 8 Ma. In the Aiguilles Rouges massif, the cooling initiated at 18 +/− 1 Ma. The AR massif cooling rate was constant at 5–15 °C Ma^{-1} since the onset of exhumation and until 8 Ma. We propose that the onset of cooling of the MB and AR massifs reflects the onset of their exhumation above frontal crustal ramps connected to the Subalpine Molasse Thrust and external fold-and-thrust-belts.

As for other ECM in the Western Alps, collisional deformation propagated in-sequence. The ECM experienced significant internal shortening at their metamorphic peak before their cooling and exhumation controlled by frontal crustal-scale thrust ramps.

Acknowledgements

The authors thank C. Rosenberg for discussions during fieldtrip, B. Tibari for (U–Th–Sm)/He analysis, A. Vitale-Brovarone and O. Beyssac for their help on RSCM analysis. J. von Raumer is acknowledged for his constructive review that helped at improving the manuscript. Thanks are due to J. P. Avouac for editorial handling. This study was funded by the INSU-Syster program (2010 − 2011).

References

Ayrton, S., Barféty, J.C., Bellière, J., Gubler, Y., Jemelin, L., 1987. Carte géologique de Chamonix (1/50 000). B.R.G.M., orléans.

Bauville, A., Epard, J.-L., Schmalholz, S.M., 2013. A simple thermo-mechanical shear model applied to the Morcles fold nappe (Western Alps). Tectonophysics 583, 76–87. http://dx.doi.org/10.1016/j.tecto.2012.10.022.

Becker, A., 2000. The Jura Mountains — an active foreland fold-and-thrust-belt? Tectoophysics 321, 381–406. http://dx.doi.org/10.1016/S0040-1951(00)00089-5.

Bellahsen, N., Jolivet, L., Lacombe, O., Bellanger, M., Boutoux, A., Garcia, S., Mouthereau, F., Le Pourhiet, L., Gumiaux, C., 2012. Mechanisms of margin inversion in the external Western Alps: implications for crustal rheology. Tectonophysics 560-561, 62–83. http://dx.doi.org/10.1016/j.tecto.2012.06.022.

Bellahsen, N., Mouthereau, F., Boutoux, A., Bellanger, M., Lacombe, O., Jolivet, L., Rolland, Y., 2014. Collision kinematics in the western external Alps. Tectonics 33, 1–34. http://dx.doi.org/10.1002/2013TC003453.

Bellanger, M., Bellahsen, N., Jolivet, L., Baudin, T., Augier, R., Boutoux, A., 2014. Basement shear zones development and shortening kinematics in the Ecrins Massif, Western Alps. Tectonics 33, 84–111. http://dx.doi.org/10.1002/2013TC003294.

Bellanger, M., Augier, R., Bellahsen, N., Jolivet, L., Monié, P., Baudin, T., Beyssac, O., 2015. Shortening of the European Dauphinois margin (Oisans Massif, Western Alps): new insights from RSCM maximum temperature estimates and 40Ar/39Ar in situ dating. J. Geodyn. 83, 37–64. http://dx.doi.org/10.1016/j.jog.2014.09.004.

Bernet, M., 2009. A field-based estimate of the zircon fission-track closure temperature. Chem. Geol. 259, 181–189. http://dx.doi.org/10.1016/j.chemgeo.2008.10.043.

Bertini, G., Marcucci, M., Nevini, R., Passerini, P., Sguazzoni, G., 1985. Patterns of faulting in the Mont Blanc granite. Tectonophysics 111, 65–106.

Beyssac, O., Rouzaud, J.-N., Goffé, B., Brunet, F., Chopin, C., 2002a. Graphitization in a high-pressure, low-temperature metamorphic gradient: a Raman microspectroscopy and HRTEM study. Contrib. Mineral. Petrol. 143 (1), 19–31. http://dx.doi.org/10.1007/s00410-001-0324-7.

Beyssac, O., Goffé, B., Chopin, C., Rouzaud, J.N., 2002b. Raman spectra of carbonaceous material in metasediments: a new geothermometer. J. Metamorph. Geol. 20 (9), 859–871. http://dx.doi.org/10.1046/j.1525-1314.2002.00408.x.

Beyssac, O., Brunet, F., Petitet, J.-P., Goffé, B., Rouzaud, J.-N., 2003. Experimental study of the microtextural and structural transformations of carbonaceous materials under pressure and temperature. Eur. J. Mineral. 15, 937–951. http://dx.doi.org/10.1127/0935-1221/2003/0015-0937.

Boutoux, A., Bellahsen, N., Lacombe, O., Verlaguet, A., Mouthereau, F., 2014. Inversion of pre-orogenic extensional basins in the external Western Alps: Structure, microstructures and restoration. J. Struct. Geol. 60, 13–29. http://dx.doi.org/10.1016/j.jsg.2013.12.014.

Brändlein, P., Nollau, G., Sharp, Z., von Raumer, J., 1994. Petrography and geochemistry of theVallorcine-Granite (Aiguilles-RougesMassif, western Alps). Schweiz. Mineral. Petrogr. Mitt. 74, 227–243.

Burkhard, M., Goy-Eggenberger, D., 2001. Near vertical isoillite-crystallinity surfaces cross-cut the recumbent fold structure of the Morcles nappe, Swiss Alps. Clay Miner. 36, 159–170.

Burkhard, M., 1988. L'Helvétique de la bordure occidentale du massif de l'Aar (évolution tectonique et métamorphique). Eclogae Geol. Helv. 81, 63–114. http://dx.doi.org/10.5169/seals-166171.

Burkhard, M., Sommaruga, A., 1998. Evolution of the western Swiss Molasse basin: structural relations with the Alps and the Jura belt. In Cenozoic Foreland Basins of Western Europe. Geol. Soc. Lond., Spec. Publ. 134, 279–298. http://dx.doi.org/10.144/GSL.SP.1998.134.013.

Bussy, F., von Raumer, J.F., 1994. U–Pb geochronology of Palaeozoic magmatic events in the Mont-Blanc Crystalline Massif, Western Alps. Schweiz. Mineral. Petrogr. Mitt. 74, 514–515.

Bussy, F., Hernandez, J., von Raumer, J., 2000. Bimodal magmatism as a consequence of the post-collisional readjustment of the thickened Variscan continental lithosphere (Aiguilles Rouges–Mont Blanc Massifs, Western Alps). Transaction of the Royal Sosciety of Edinburgh. Earth Sci. 91 (1–2), 221–233. http://dx.doi.org/10.1017/S0263593300007392.

Butler, R.W.H., Tavarnelli, E., Grasso, M., 2006. Structural inheritance in mountain belts: an Alpine–Apennine perspective. J. Struct. Geol. 28, 1893–1908. http://dx.doi.org/10.1016/j.jsg.2006.09.006.

Cenki-Tok, B., Darling, J.R., Rolland, Y., Dhuime, B., Storey, C.D., 2013. Direct dating of mid-crustal shear zones with synkinematic allanite: new in situ U–Th–Pb geochronological approaches applied to the Mont Blanc massif. Terra Nova 26, 29–37. http://dx.doi.org/10.1111/ter.12066.

Challandes, N., Marquer, D., Villa, I.M., 2008. P–T–t modelling, fluid circulation, and 39Ar–40Ar and Rb–Sr mica ages in the Aar Massif shear zones (Swiss Alps). Swiss J. Geosci. 101, 269–288. http://dx.doi.org/10.1007/s00015-008-1260-6.

Crespo-Blanc, A., Masson, H., Sharp, Z.D., Cosca, M.A., Hunziker, J.C., 1995. A stable and 40Ar/39Ar isotope study of a major thrust in the Helvetic nappes (Swiss Alps): evidence for fluid flow and constraints on nappe kinematics. Geol. Soc. Am. Bull. 107, 1129–1144. http://dx.doi.org/10.1130/0016-7606(1995)107<1129.

Crouzet, C., Ménard, G., Rochette, P., 2001. Cooling history of the Dauphinoise Zone (Western Alps, France) deduced from the thermopaleomagnetic record: geodynamic implications. Tectonophysics 340, 79–93. http://dx.doi.org/10.1016/S0040-1951(01)00142-1.

Egli, D., 2013. Kinematics and Timing of Alpine Deformation in the Mont Blanc region (Western Alps) (Ph-D Thesis, ETH Zurich).

Egli, D., Mancktelow, N.S., 2013. The structural history of the Mont Blanc massif with regard to models for its recent exhumation. Swiss J. Geosci. 106, 469–489. http://dx.doi.org/10.1007/s00015-013-0153-5.

Egli, D., Müller, W., Mancktelow, N., 2016. Laser-cut Rb–Sr microsampling dating of deformational events in the Mont Blanc-Aiguilles Rouges region (European Alps). Terra Nova http://dx.doi.org/10.1111/ter.12184.

Epard, J.-L., 1990. La nappe de Morcles au sud-ouest du Mont-Blanc (Ph-D Thesis) Univ. Lausanne.

Escher, A., Beaumont, C., 1997. Formation, burial and exhumation of basement nappes at crustal scale: a geometric model based on the Western Swiss-Italian Alps. J. Struct. Geol. 19, 955–974. http://dx.doi.org/10.1016/S0191-8141(97)00022-9.

Escher, A., Masson, H., Steck, A., 1993. Nappe geometry in the western Swiss Alps. J. Struct. Geol. 15, 501–509.

Fabre, C., Boiron, M.C., Dubessy, J., Cathelineau, M., Banks, D.A., 2002. Palaeofluid chemistry of a single fluid event: a bulk and in-situ multi-technique analysis (LIBS, Raman Spectroscopy) of an Alpine fluid (Mont-Blanc). Chem. Geol. 182, 249–264.

Farley, K.a., 2000. Helium diffusion from apatite: General behavior as illustrated by Durango fluorapatite. J. Geophys. Res. 105, 2903–2914. http://dx.doi.org/10.1029/1999JB900348.

Ford, M., Duchêne, S., Gasquet, D., Vanderhaeghe, O., 2006. Two-phase orogenic convergence in the external and internal SW Alps. J. Geol. Soc. Lond. 163, 815–826. http://dx.doi.org/10.1144/0016-76492005-034.

Frey, M., Desmons, J., Neubauer, F., 1999. The new Metamorphic map of the Alps. Schweizerische Mineralogische und Petrographische Mitteilungen, 79/1. Stäubli Verlag AG, Zürich (230 pp.).

Fügenschuh, B., Schmid, S.M., 2003. Late stages of deformation and exhumation of an orogen constrained by fission-track data: a case study in the Western Alps. Geol. Soc. Am. Bull. 115, 1425–1440. http://dx.doi.org/10.1130/B25092.1.

Gallagher, K., Brown, R., Johnson, C., 1998. Fission track analysis and its applications to geological problems. Annu. Rev. Earth Planet. Sci. 26, 519–572. http://dx.doi.org/10.1146/annurev.earth.26.1.519.

Garver, A.J.I., Reiners, P.W., Walker, L.J., Ramage, J.M., Perry, S.E., 2005. Implications for timing of Andean uplift from thermal resetting of radiation-damaged zircon in the Cordillera Huayhuash, Northern Peru. J. Geol. 113, 117–138. http://dx.doi.org/10.1086/427664.

Glotzbach, C., Reinecker, J., Danišík, M., Rahn, M., Frisch, W., Spiegel, C., 2008. Neogene exhumation history of the Mont Blanc massif, western Alps. Tectonics 27, TC4011. http://dx.doi.org/10.1029/2008TC002257.

Glotzbach, C., Reinecker, J., Danišík, M., Rahn, M.K., Frisch, W., Spiegel, C., 2010. Thermal history of the central Gotthard and Aar massifs, European Alps: Evidence for steady state, long-term exhumation. J. Geophys. Res. 115, F03017. http://dx.doi.org/10.1029/2009JF001304.

Glotzbach, C., van der Beek, P.A., Spiegel, C., 2011. Episodic exhumation and relief growth in the Mont Blanc massif, Western Alps from numerical modelling of thermochronology data. Earth Planet. Sci. Lett. 304, 417–430. http://dx.doi.org/10.1016/j.epsl.2011.02.020.

Godard, V., Pik, R., Lavé, J., Cattin, R., Tibari, B., de Sigoyer, J., Pubellier, M., Zhu, J., 2009. Late Cenozoic evolution of the central Longmen Shan, eastern Tibet: Insight from (U–Th)/He thermochronometry. Tectonics 28, TC5009. http://dx.doi.org/10.1029/2008TC002407.

Guellec, S., Lajat, D., Mascle, A., Roure, F., Tardy, M., 1990. Deep seismic profiling and petroleum potential in the western Alps: constraints with ECORS data, balanced cross-sections and hydrocarbon modeling. The Potential of Deep Seismic Profiling for Hydrocarbon Exploration. Edition Technip, Paris, pp. 425–437.

Guenthner, W.R., Reiners, P.W., Ketcham, R.A., Nasdala, L., Giester, G., 2013. Helium diffusion in natural zircon: radiation damage, anisotropy, and the interpretation of zircon (U–Th)/He thermochronology. Am. J. Sci. 313, 145–198. http://dx.doi.org/10.2475/03.2013.01.

Ketcham, R.A., 2005. Forward and inverse modeling of low-temperature thermochronometry data. Rev. Mineral. Geochem. 58, 275–314. http://dx.doi.org/10.2138/rmg.2005.58.11.

Ketcham, R.A., Gautheron, C., Tassan-Got, L., 2011. Accounting for long alpha-particle stopping distances in (U–Th–Sm)/He geochronology: refinement of the baseline case. Geochim. Cosmochim. Acta 75, 7779–7791. http://dx.doi.org/10.1016/j.gca.2011.10.011.

Kirschner, D.L., Sharp, Z.D., Masson, H., 1995. Oxygen isotope thermometry of quartz-calcite veins: Unraveling the thermal-tectonic history of the subgreenschist facies Morcles nappe (Swiss Alps). Geol. Soc. Am. Bull. 107, 1145–1156. http://dx.doi.org/10.1130/0016-7606(1995)107<1145.

Kirschner, D.L., Masson, H., Cosca, M.A., 2003. An 40 Ar/ 39 Ar, Rb/Sr, and stable isotope study of micas in low-grade fold-and-thrust belt: an example from the Swiss Helvetic Alps. Contrib. Mineral. Petrol. 145, 460–480. http://dx.doi.org/10.1007/s00410-003-0461-2.

Lacombe, O., Mouthereau, F., 2002. Basement-involved shortening and deep detachment tectonics in forelands of orogens: insights from recent collision belts (Taiwan, Western Alps, Pyrenees). Tectonics 21, 12-1–12-22. http://dx.doi.org/10.1029/2001TC901018.

Lahfid, A., Beyssac, O., Deville, E., Negro, F., Chopin, C., Goffé, B., 2010. Evolution of the Raman spectrum of carbonaceous material in low-grade metasediments of the Glarus Alps (Switzerland). Terra Nova 22 (5), 354–360. http://dx.doi.org/10.1111/j.13653121.2010.00956.x.

Leloup, P.H., Arnaud, N., Sobel, E.R., Lacassin, R., 2005. Alpine thermal and structural evolution of the highest external crystalline massif: the Mont Blanc. Tectonics 24, TC4002. http://dx.doi.org/10.1029/2004TC001676.

Mouthereau, F., Watts, A.B., Burov, E., 2013. Structure of orogenic belts controlled by lithosphere age. Nat. Geosci. 6, 785–789. http://dx.doi.org/10.1038/ngeo1902.

Mullis, J., 1975. Growth conditions of Quartz Crystals from Val d'Illiez (Valais, Switzerland). Schweizerische Mineral. und Petrogr. Mitteilungen 55, 419–429.

Nicolas, A., Hirn, A., Nicolich, R., Polino, R., 1990. Lithospheric wedging in the western Alps inferred from the ECORS-CROP traverse. Geology 18 (7), 587–590.

Pik, R., Marty, B., Carignan, J., Lavé, J., 2003. Stability of the Upper Nile drainage network (Ethiopia) deduced from (U–Th)/He thermochronometry: implications for uplift and erosion of the Afar plume dome. Earth Planet. Sci. Lett. 215, 73–88. http://dx.doi.org/10.1016/S0012-821X(03)00457-6.

Poty, B., Stadler, H.A., Weisbrod, A.M., 1974. Fluid inclusion studies in quartz from fissures of the Western and Central Alps. Schweiz. Mineral. Petrogr. Mitt. 54, 717–752.

Rahn, M.K., 1994. Incipient Metamorphism of the Glarus Alps: Petrology of the Taveyanne Greywacke and Fission Track Dating (Ph-D Thesis) Univ. of Basel, Basel, Switzerland.

Rahn, M.K., Brandon, M.T., Batt, G.E., Garver, J.I., 2004. A zero-damage model for fission-track annealing in zircon. Am. Mineralineralogist 89, 473–484.

Ramsay, J.G., Casey, M., Kligfield, R., 1983. Role of shear in development of the Helvetic fold-thrust belt of Switzerland. Geology 11, 439–442. http://dx.doi.org/10.1130/0091-7613(1983)11<439:ROSIDO>2.0.CO;2.

Reiners, P.W., Farley, K.A., Hickes, H.J., 2002. He diffusion and (U-Th)/He thermochronometry of zircon: Initial results from Fish Canyon Tuff and Gold Butte. Tectonophysics 349, 297–308. http://dx.doi.org/10.1016/S0040-1951(02)00058-6.

Reiners, P.W., Thomson, S.N., McPhillips, D., Donelick, R.A., Roering, J.J., 2007. Wildfire thermochronology and the fate and transport of apatite in hillslope and fluvial environments. J. Geophys. Res. 112, F04001. http://dx.doi.org/10.1029/2007JF000759.

Rolland, Y., Rossi, M., 2016. Two-stage fluid flow and element transfer in shear zones during collision burial–exhumation cycle: insights from the Mont Blanc Crystalline Massif (Western Alps). J. Geodyn. http://dx.doi.org/10.1016/j.jog.2016.03.016.

Rolland, Y., Cox, S.F., Boullier, A.-M., Pennacchioni, G., Mancktelow, N.S., 2003. Rare earth and trace element mobility in mid-crustal shear zones: insights from the Mont Blanc Massif (Western Alps). Earth Planet. Sci. Lett. 214, 203–219. http://dx.doi.org/10.1016/S0012-821X(03)00372-8.

Rolland, Y., Corsini, M., Rossi, M., Cox, S.F., Pennacchioni, G., Mancktelow, N., Boullier, A.M., 2007. Comment on the dating of Alpine deformation by Ar–Ar on syn-kinematic mica in mid-crustal shear zones of the Mont Blanc Massif (paper by Leloup et al.). Tectonics 26, TC2015. http://dx.doi.org/10.1029/2006TC001956.

Rolland, Y., Rossi, M., Cox, S.F., Corsini, M., Mancktelow, N.S., Pennacchioni, G., Fornari, M., Boullier, A., 2008. 40Ar/39Ar dating of synkinematic white mica: insights from fluid-rock reaction in low-grade shear zones (Mont Blanc Massif) and constraints on timing of deformation in the NW external Alps. Geol. Soc. Lond., Spec. Publ. 299, 293–315. http://dx.doi.org/10.1144/SP299.18.

Rolland, Y., Cox, S.F., Corsini, M., 2009. Constraining deformation stages in brittle–ductile shear zones from combined field mapping and 40Ar/39Ar dating: The structural evolution of the Grimsel Pass area (Aar Massif, Swiss Alps). J. Struct. Geol. 31, 1377–1394.

Rossi, M., Rolland, Y., 2014. Stable isotope and Ar-Ar evidence of prolonged multi-scale fluid flow during exhumation of orogenic crust: example from the Mont Blanc and Aar massifs (NW Alps). Tectonics 33 (9), 1681–1709.

Rossi, M., Rolland, Y., Vidal, O., Cox, S.F., 2005. Geochemical variations and element transfer during shear zone development and related episyenites at middle crust depths: insights from the study of the Mont-Blanc Granite (French–Italian Alps). Geol. Soc. Lond. Spec. Publ. 245, 373–396.

Ruffini, R., Polino, R., Cosca, M.A., Hunziker, J., Masson, H., 1993. New data on Taveyanne-related volcanic activity. Plinius 10, 223–224.

Sanchez, G., Rolland, Y., Schneider, J., Corsini, M., Oliot, E., Goncalves, P., Verati, C., Lardeaux, J.-M., Marquer, D., 2001. Dating low-temperature deformation by 40Ar/39Ar on white mica, insights from the Argentera-Mercantour Massif (SW Alps). Lithos 125, 521–536. http://dx.doi.org/10.1016/j.lithos.2011.03.009.

Schmid, S.M., Pfiffner, O.A., Froitzheim, N., Schönborn, G., Kissling, E., 1996. Geophysical-geological transect and tectonic evolution of the Swiss-Italian Alps. Tectonics 15, 1036–1064. http://dx.doi.org/10.1029/96TC00433.

Seward, D., Mancktelow, N.S., 1994. Neogene kinematics of the central and western Alps: evidence from fission-track dating. Geology 22, 803–806. http://dx.doi.org/10.1130/0091-7613(1994)022<0803:NKOTCA>2.3.CO;2.

Sharp, Z.D., Kirschner, D.L., 1994. Quartz-calcite oxygen isotope thermometry: a calibration based on natural isotopic variations. Geochim. Cosmochim. Acta 58 (21), 4491–4501. http://dx.doi.org/10.1016/0016-7037(94)90350-6.

Shuster, D.L., Farley, K.A., 2009. The influence of artificial radiation damage and thermal annealing on helium diffusion kinetics in apatite. Geochim. Cosmochim. Acta 73, 183–196. http://dx.doi.org/10.1016/j.gca.2008.10.013.

Simon-Labric, T., Rolland, Y., Dumont, T., Heymes, T., Authemayou, C., Corsini, M., Fornari, M., 2009. 40Ar/39Ar dating of Penninic Front tectonic displacement (W Alps) during the Lower Oligocene (31–34 Ma). Terra Nova 21, 127–136.

Sinclair, H.D., 1997. Tectonostratigraphic model for underfilled peripheral foreland basins: an Alpine perspective. Geol. Soc. Am. Bull. 109, 324–346.

Soom, M.A., 1990. Abkiihlungs—und Hebungsgeschichte der Extemmas—sive und der penninischen Decken beidseits der Simplon-Rhone-Linie seit dem Oligoziin: Spaltspurdatierungen an Apatit/Zircon und K–Ar—Datierungen an Biotit/Muskowit (Westliche Zentralalpen) (Ph-D Thesis) University of Bern, Switzerland.

Steck, A., Epard, J.L., Escher, A., Lehner, P., Marchant, R., Masson, H., 1997. Geological interpretation of the seismic profiles through western Switzerland: Rawil (W1), Val d'Anniviers (W2), Mattertal (W3), Zmutt-Zermatt-Findelen (W4) and Val de Bagnes (W5). In: Pfiffner, O.A., et al. (Eds.), Deep Structure of the Swiss Alps: Results from NRP 20. Birkhäuser Verlag, Basel: Boston, pp. 123–138.

Stockli, D.F., 2005. Application of Low-Temperature Thermochronometry to Extensional Tectonic Settings. Rev. Mineral. Geochemistry 58, 411–448. http://dx.doi.org/10.2138/rmg.2005.58.16.

Tibari, B., Vacherat, A., Stab, M., Pik, R., Yeghicheyan, D., Hild, P., 2016. An Alternative Protocol for Single Zircon Dissolution with Application to (U-Th-Sm)/He Thermochronometry. Geostand. Geoanalytical Res. http://dx.doi.org/10.1111/j.1751-908X.2016.00375.x.

Vacherat, A., Mouthereau, F., Pik, R., Bernet, M., Gautheron, C., Masini, E., Le Pourhiet, L., Tibari, B., Lahfid, A., 2014. Thermal imprint of rift-related processes in orogens as recorded in the Pyrenees. Earth Planet. Sci. Lett. 408, 296–306. http://dx.doi.org/10.1016/j.epsl.2014.10.014.

Valla, P.G., van der Beek, P.A., Shuster, D.L., Braun, J., Herman, F., Tassan-Got, L., Gautheron, C., 2012. Late Neogene exhumation and relief development of the Aar and Aiguilles Rouges massifs (Swiss Alps) from low-temperature thermochronology modeling and 4He/3He thermochronometry. J. Geophys. Res. 117, F01004. http://dx.doi.org/10.1029/2011JF002043.

Van der Beek, P.A., Valla, P.G., Herman, F., Braun, J., Persano, C., Dobson, K.J., Labrin, E., 2010. Inversion of thermochronological age–elevation profiles to extract independent estimates of denudation and relief history. II: Application to the French Western Alps. Earth Planet. Sci. Lett. 296, 9–22. http://dx.doi.org/10.1016/j.epsl.2010.04.032.

Vernon, A.J., van der Beek, P.A., Sinclair, H.D., Rahn, M.K., 2008. Increase in late Neogene denudation of the European Alps confirmed by analysis of a fission-track thermochronology database. Earth Planet. Sci. Lett. 270, 316–329. http://dx.doi.org/10.1016/j.epsl.2008.03.053.

von Raumer, J.F., Bussy, F., 2004. Mont-Blanc and Aiguilles-Rouges: geology of their polymetamorphic basement (External massifs, France-Switzerland). Mémoires de Géologie (Lausanne) 42, 1–203.

von Raumer, J., Bussy, F., Stampfli, G., 2009. The Variscan evolution in the Alps – and place in their Variscan framework. Comptes Rendus de l'Académie des Sciences, Geosciences, Paris 341, 239–252.

Whipple, K.X., Meade, B.J., 2006. Orogen response to changes in climatic and tectonic forcing. Earth Planet. Sci. Lett. 243, 218–228. http://dx.doi.org/10.1016/j.epsl.2005.12.022.

Yui, T.-F., Huang, E., Xu, J., 1996. Raman spectrum of carbonaceous material: a possible metamorphic grade indicator for low-grade metamorphic rocks. J. Metamorph. Geol. 14 (2), 115–124. http://dx.doi.org/10.1046/j.15251314.1996.05792.x.